Replication

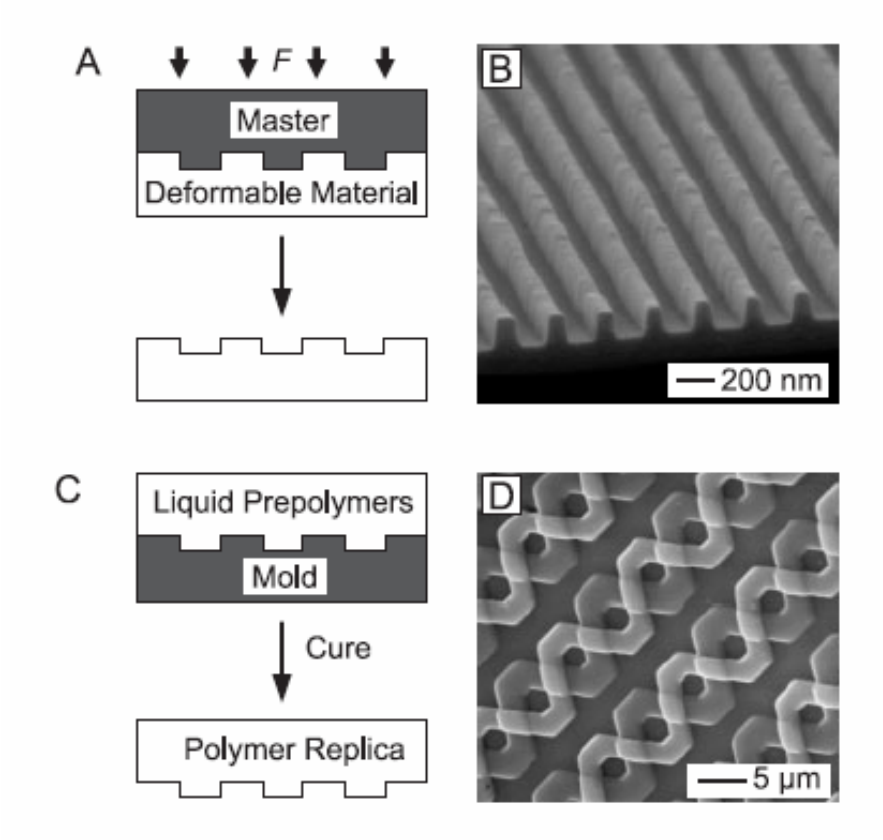

Align the pattern and Exposure

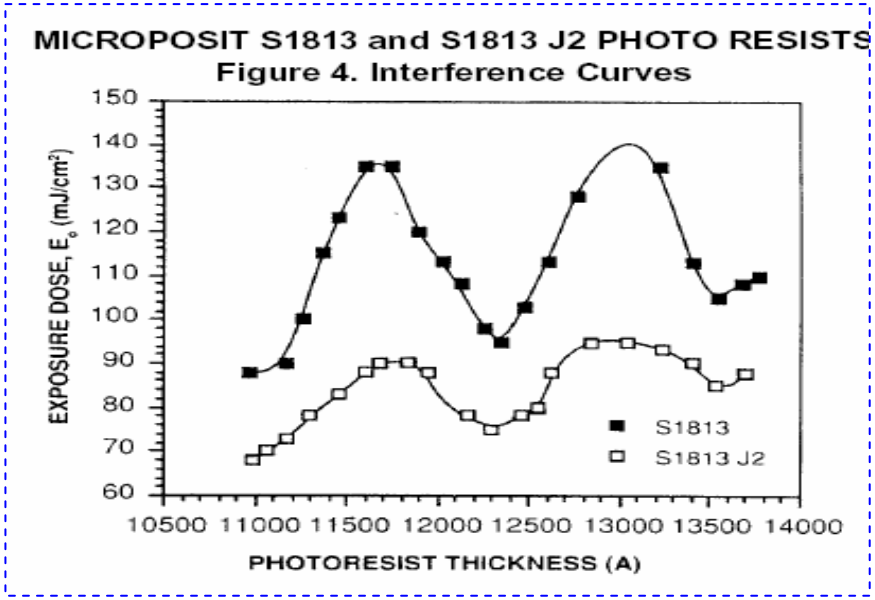

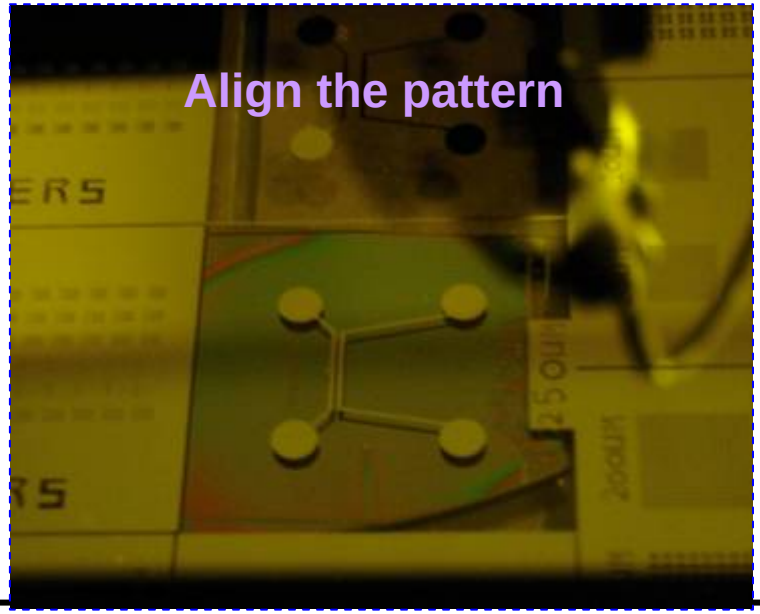

Stepper

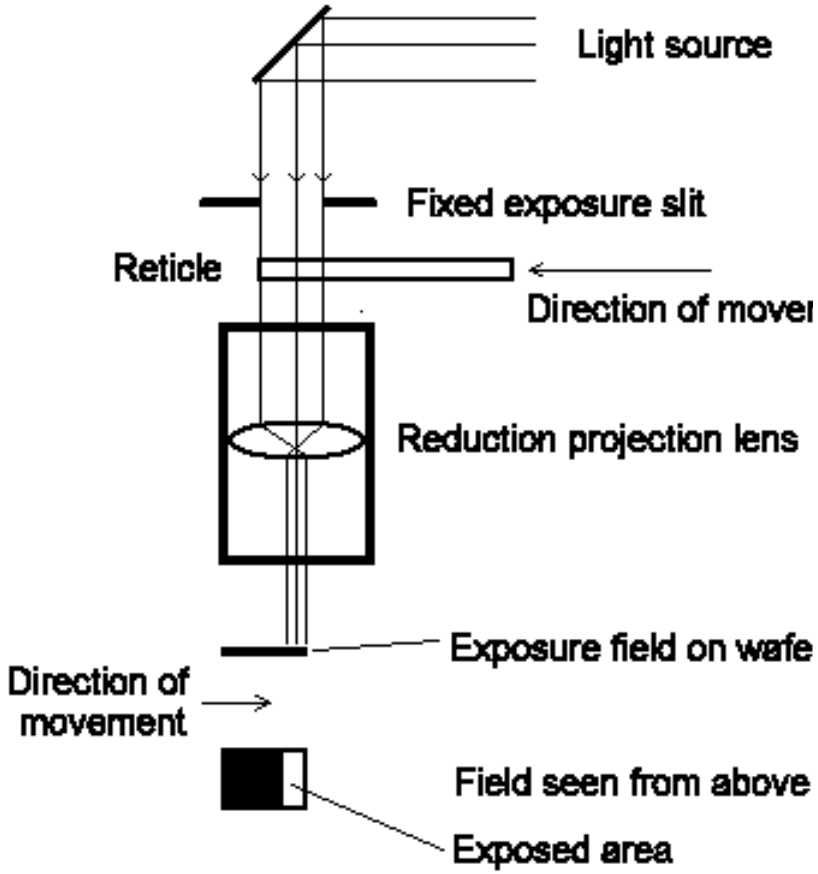
Light source
Fixed exposure slit
Reticle
Direction of move
Reduction projection lens
Exposure field on wafe
Direction of movement
Field seen from above
Exposed area

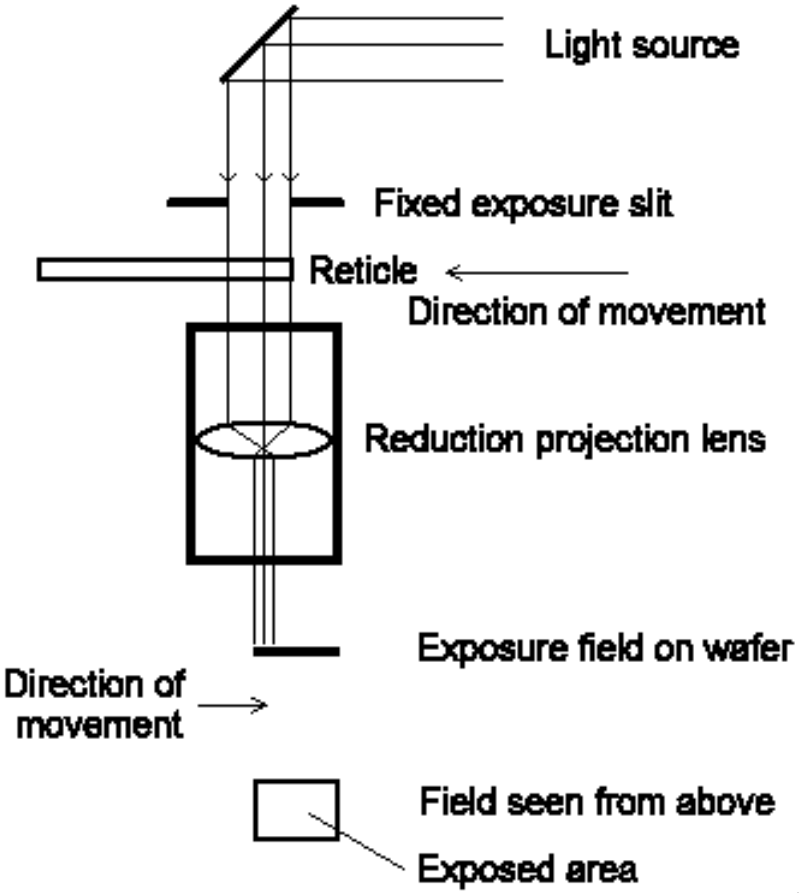
Light source
Fixed exposure slit
Reticle
Direction of movement
Reduction projection lens
Exposure field on wafer
Direction of movement
Field seen from above
Exposed area

E-beam Projection

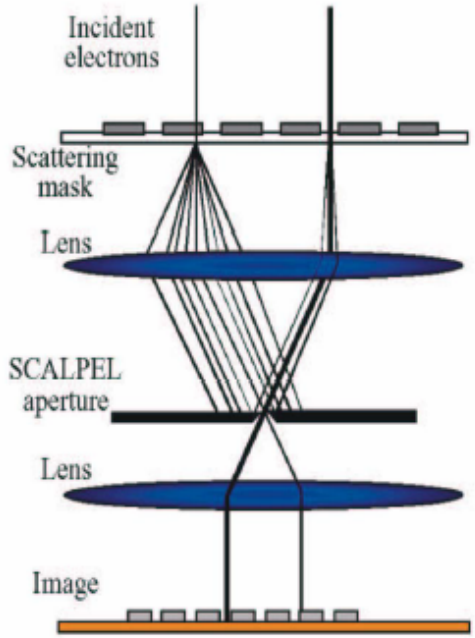

Bell Lab (1999)
There 'was' a consortium including Applied Materials, Inc. and ASM Lithography Holding N.V.; Lucent Technologies Inc.; Motorola, Semiconductor Products Sector; Samsung Electronics Co., Ltd.; and Texas Instruments Incorporated (TI).

Imprint Lithography with 25-Nanometer Resolution

Stephen Y. Chou; Peter R. Krauss; Preston J. Renstrom

Science, New Series, Volume 272, Issue 5258 (Apr. 5, 1996), 85-87.

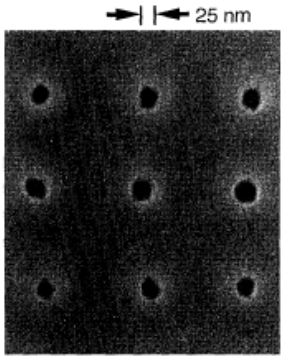

Fig. 2. SEM micrograph of a top view of holes 25 nm in diameter with a period of 120 nm, formed by compression molding into a PMMA film.

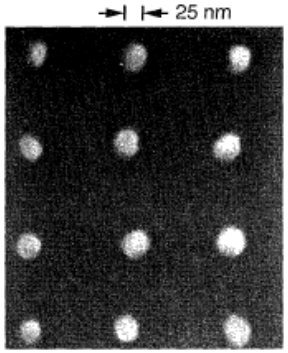

Fig. 5. SEM micrograph of the substrate in Fig. 2, after deposition of metal and a lift-off process. The diameter of the metal dots is 25 nm, the same as that of the original holes created in the PMMA.

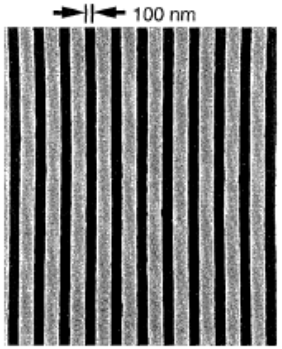

Fig. 3. SEM micrograph of a top view of trenches 100 nm wide with a period of 250 nm, formed by compression molding into a PMMA film.

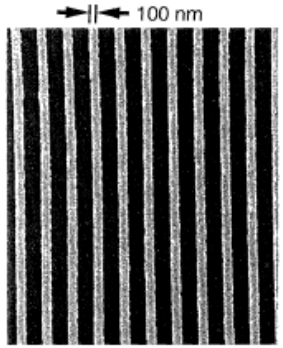

Fig. 6. SEM micrograph of the substrate in Fig. 3, after deposition of metal and a lift-off process. The metal linewidth is 100 nm, the same as the width of the original PMMA trenches.

Nanoimprint Lithography

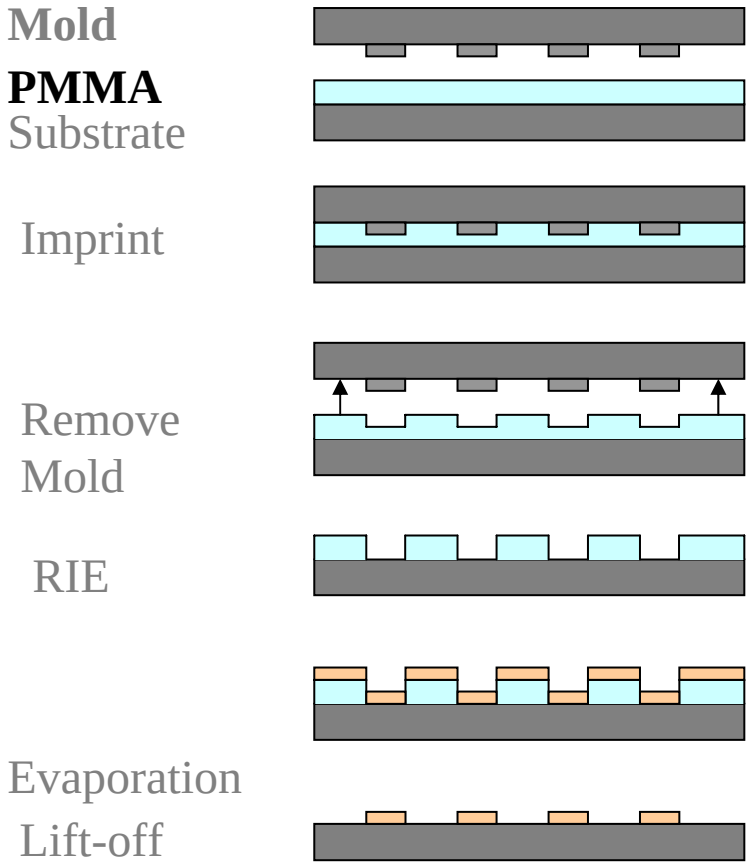

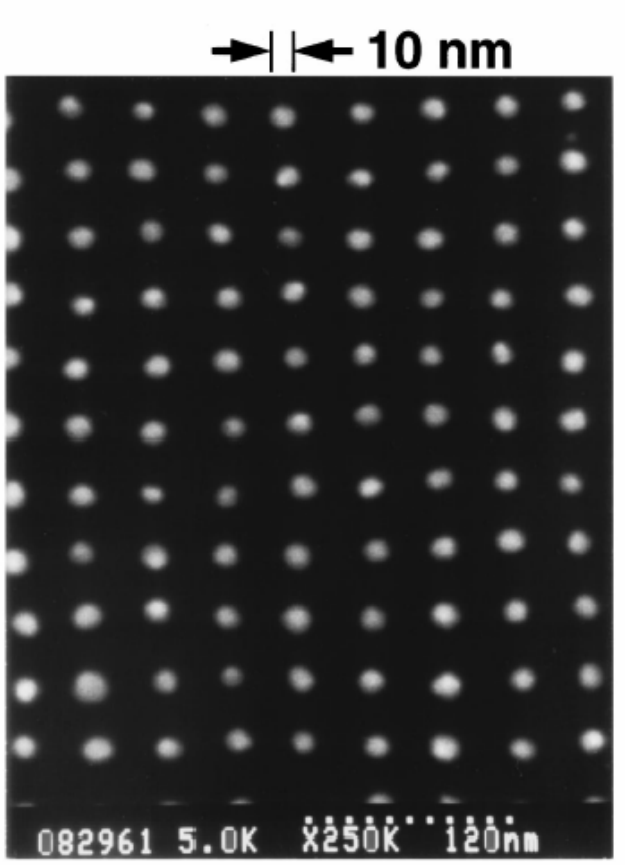

Ultrafast and direct imprint of nanostructures in silicon

NATURE | VOL 417 | 20 JUNE 2002 |

Stephen Y. Chou*, Chris Keimel & Jian Gu

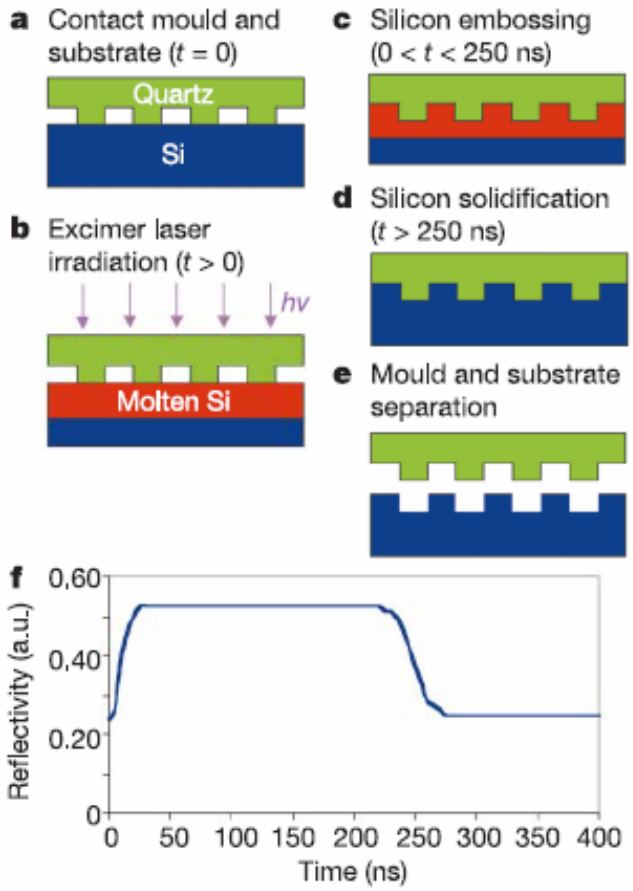

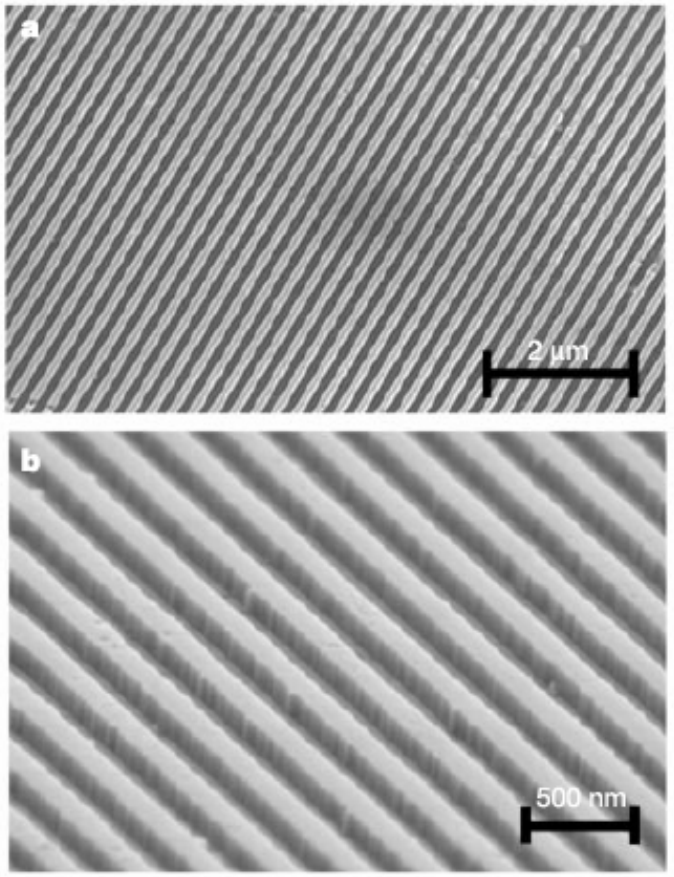

Step and Flash Imprint Lithography

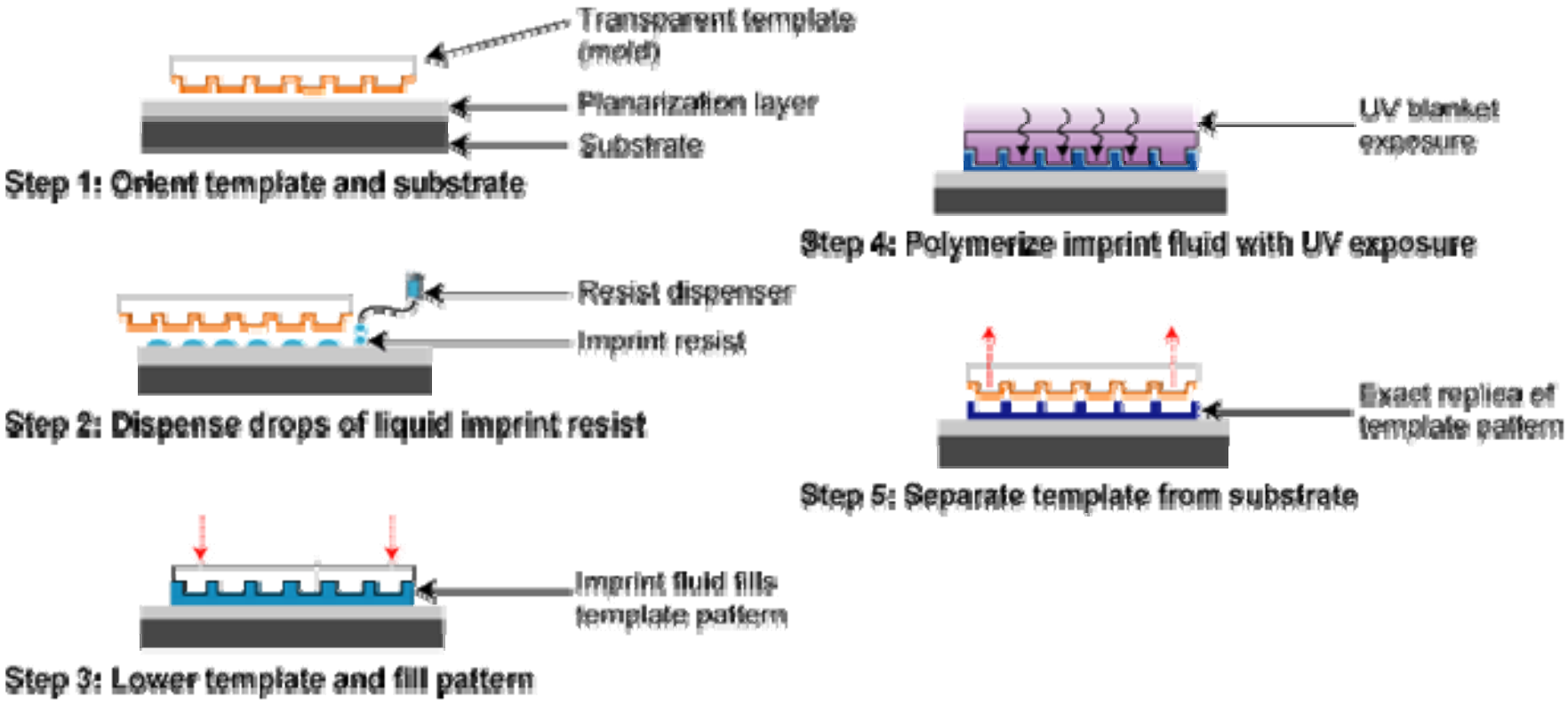

Nanoimprintors

NX-2000, Nanoimprintor, Nanonex

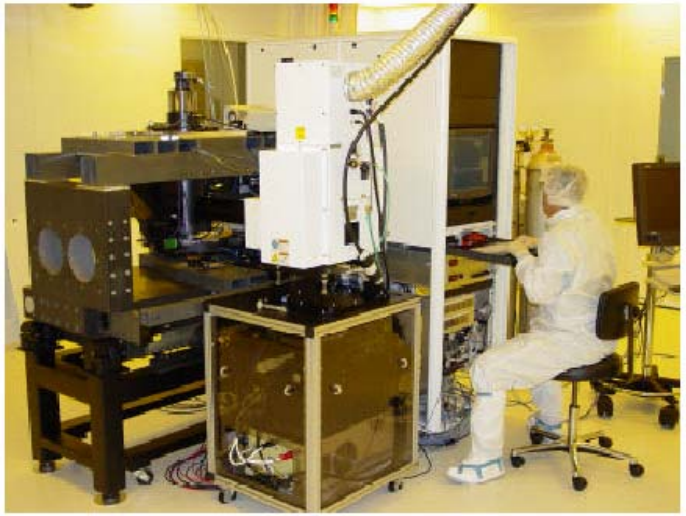

IMPRIO 100

Molecular Imprints, Inc.™

- Resolution: Sub-50 nanometers, imprint template (mold) limited.
- Alignment: < 500 nm, 3σ (X, Y, and Rotation).
- Flexibility: Handles up to 8 inch wafers, including fragile substrates.
- Field size: 25 x 25 mm full active print area, 100 μm street width.

Imprinting Result

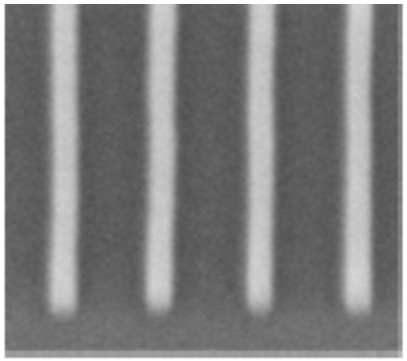

Imprinted 20 nm isolated lines

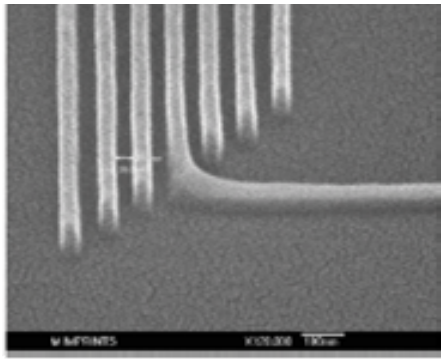

Imprinted 30 nm dense lines

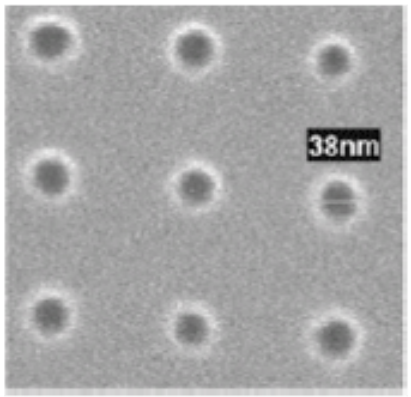

Imprinted sub-40 nm contacts

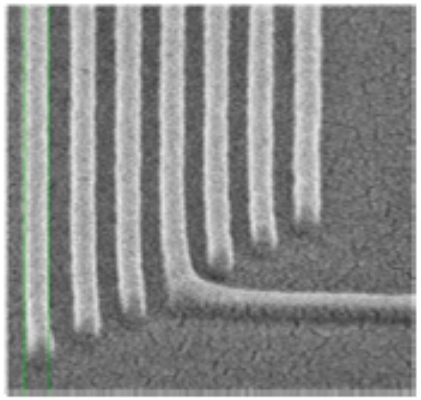

Imprinted 50 nm dense lines

Challenges

- Mask Fabrication (1:1)
- Lift-off process
- Resist
- Mask Design

Soft Lithography

Annu. Rev. Mater. Sci. 1998. 28:153–84

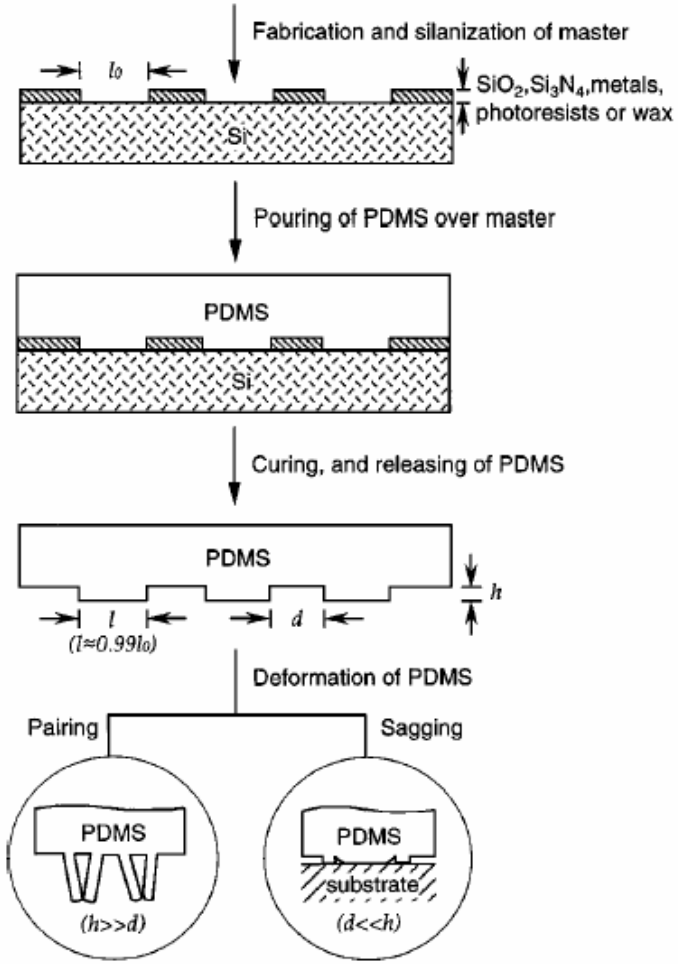

Soft Lithography

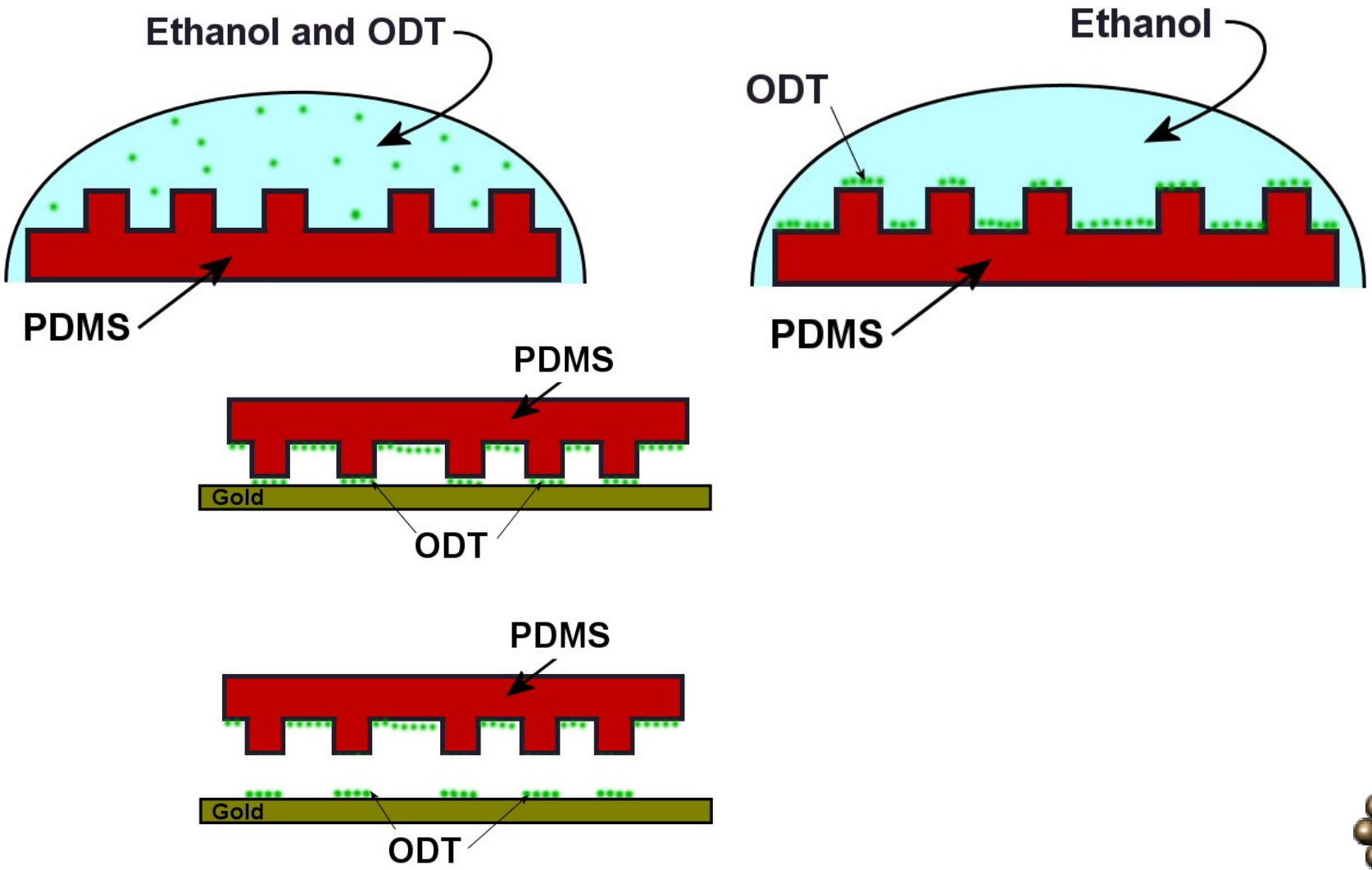

Table 1 Comparison between photolithography and soft lithography

	Photolithography	Soft lithography
Definition of patterns	Rigid photomask (patterned Cr supported on a quartz plate)	Elastomeric stamp or mold (a PDMS block patterned with relief features)
Materials that can be patterned directly	Photoresists (polymers with photo-sensitive additives)	Photoresists[a,e]
	SAMs on Au and SiO_2	SAMs on Au, Ag, Cu, GaAs, Al, Pd, and SiO_2[a] Unsensitized polymers[b–e] (epoxy, PU, PMMA, ABS, CA, PS, PE, PVC) Precursor polymers[c,d] (to carbons and ceramics) Polymer beads[d] Conducting polymers[d] Colloidal materials[a,d] Sol-gel materials[c,d] Organic and inorganic salts[d] Biological macromolecules[d]
Surfaces and structures that can be patterned	Planar surfaces 2-D structures	Both planar and nonplanar Both 2-D and 3-D structures
Current limits to resolution	~250 nm (projection) ~100 nm (laboratory)	~30 nm[a,b], ~60 nm[e], ~1 μm[d,e] (laboratory)
Minimum feature size	~100 nm (?)	10 (?) - 100 nm

[a–e]Made by (a) μCP, (b) REM, (c) μTM, (d) MIMIC, (e) SAMIM. PU:polyurethane; PMMA: poly(methyl methacrylate); ABS: poly(acrylonitrile-butadiene-styrene); CA: cellulose acetate; PS: polystyrene; PE: polyethylene; and PVC: poly(vinyl chloride)

Micro-contact Printing

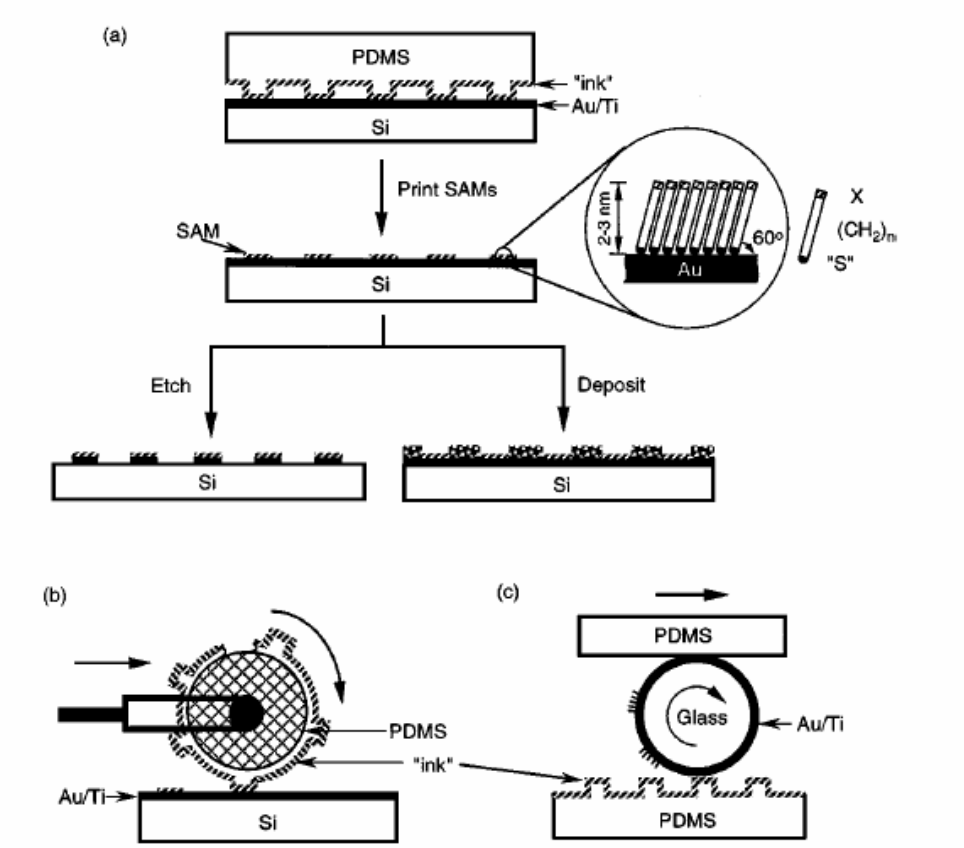

Figure 2 Schematic procedures for μCP of hexadecanethiol (HDT) on the surface of gold: (*a*) printing on a planar surface with a planar stamp (21), (*b*) printing on a planar surface over large areas with a rolling stamp (128), and (*c*) printing on a nonplanar surface with a planar stamp (174).

Micro-contact Printing

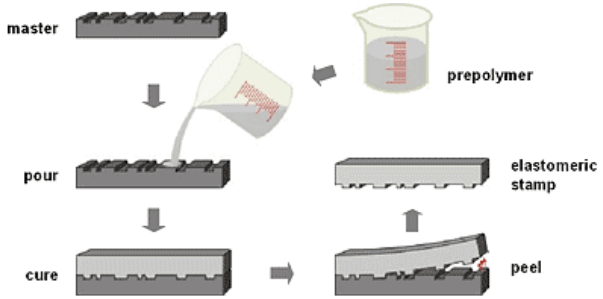

Fig.2 The stamp replication process: A master with a negative of the desired pattern is cast with a pre-polymer. After curing the polymer, the elastomeric stamp is peeled off the master and ready for microcontact printing.

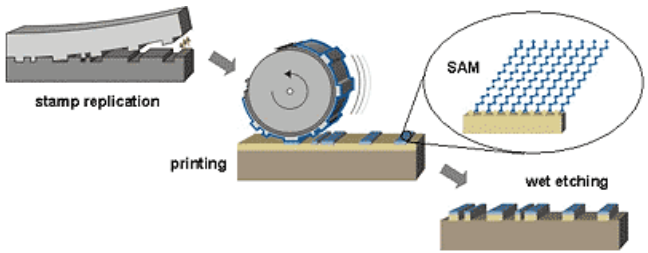

Fig.1 The microcontact printing (μCP) process: An elastomeric stamp is replicated from a master. After inking of the stamp with a suitable ink, it is fixated on a printing machine with help of which it is brought into conformal contact with a substrate. There the ink forms a self-assembled monolayer (SAM) which can be used as a resist in a subsequent wet etching step.

Micro-contact Printing

http://mrsec.wisc.edu/Edetc/nanolab/print/text.html

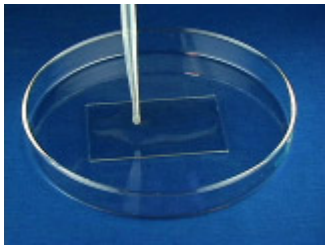

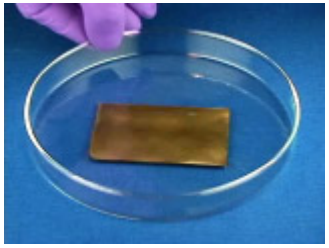

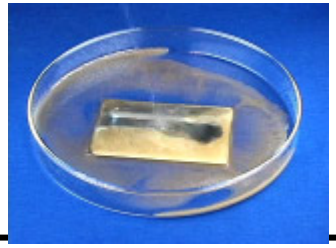

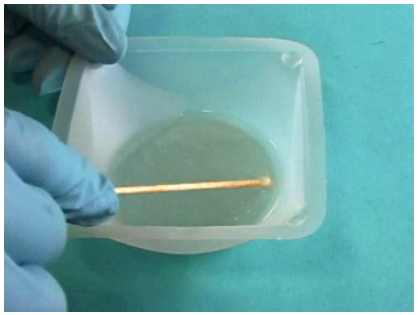

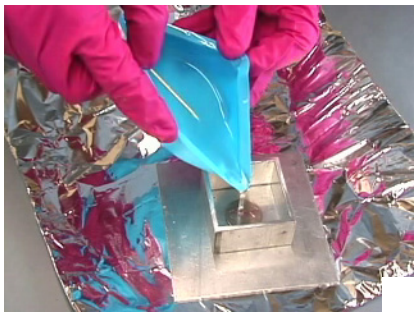

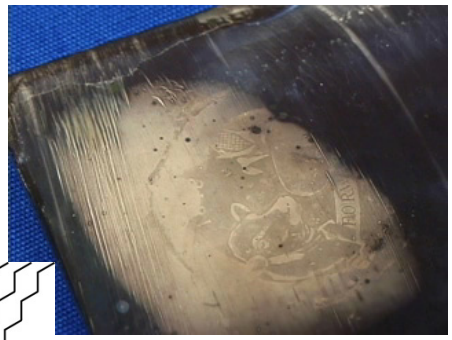

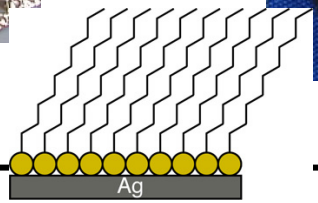

Micro-contact Printing

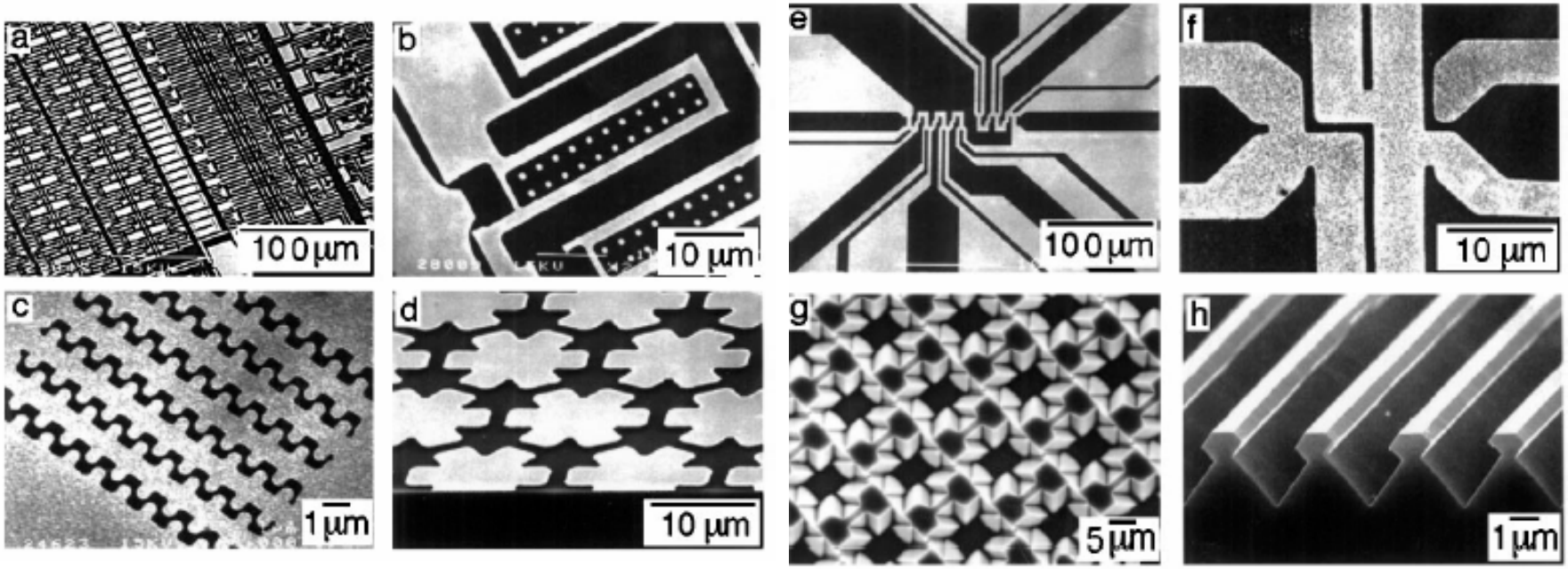

Self-Assemble Monolayer (SAM)

Chem. Rev. **2005**, *105*, 1103–1169

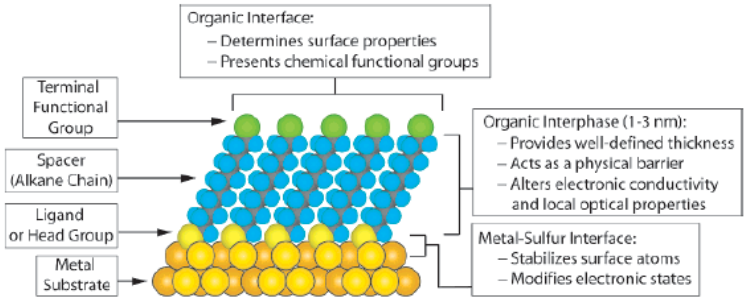

Ligand	Substrates	Morphology of Substrate: Thin Films or Bulk Material	Morphology of Substrate: Nanoparticles or Other Nanostructures
ROH	Fe_xO_y		35
	Si-H	36	
	Si	37	
RCOO-/RCOOH	α-Al_2O_3	38,39	
	Fe_xO_y		40
	Ni		41,42
	Ti/TiO_2	43	
RCOO–OOCR	Si(111):H	44	
	Si(100):H		
Ene-diol	Fe_2O_3		45
RNH_2	FeS_2	46	
	Mica	47	
	Stainless Steel 316L	48	
	$YBa_2Cu_3O_{7-\delta}$	49	
	CdSe		50
RC≡N	Ag	51	
	Au		
R-N≡N$^+$(BF_4^-)	GaAs(100)	52	
	Pd	52	
	Si(111):H	52	
RSH	Ag	26	53,54
	$Ag_{90}Ni_{10}$	55	
	AgS		56
	Au	26	57
	AuAg		58
	AuCu		58
	Au_xPd_{1-x}		58
	CdTe		59
	CdSe		60
	CdS		61,62
	Cu	26	58
	FePt		63-66
	GaAs	67	
	Ge	68	
	Hg	69-71	
	HgTe		72
	InP	73	
	Ir		74
	Ni	75	
	PbS		76-78
	Pd	30	74,79
	PdAg		58
	Pt	32	80
	Ru		81
	Stainless Steel 316L	48	
	$YBa_2Cu_3O_{7-\delta}$	82	
	Zn	83	
	ZnSe	84	
	ZnS		85
RSAc	Au	86	
R–S	Au		87
RSR'	Au	88	
RSSR'	Ag	89	90
	Au	20	90-92
	CdS		61
	Pd	30	
R–S–S	Au	93	
RCSSH	Au	94	
	CdSe		95
$RS_2O_3^-Na^+$	Au	96	98
	Cu	97	
RSeH	Ag	99	
	Au	100,101	
	CdS		60
	CdSe		102
RSeSeR'	Au	101	
R_3P	Au		103
	FeS_2	46	
	CdS		104
	CdSe		104
	CdTe		104
$R_3P=O$	Co		105,106
	CdS		104
	CdSe		104
	CdTe		104
$RPO_3^{2-}/RP(O)(OH)_2$	Al	107	
	Al-OH	108	
	$Ca_{10}(PO_4,CO_3)_6(OH)_2$	109	
	GaAs	110	
	GaN	110	
	Indium tin oxide (ITO)	111	
	Mica	112	
	TiO_2	113,114	
	ZrO_2	114,115	
	CdSe		116-118
	CdTe		118,119
RPO_4^{2-}	Al_2O_3	120	
	Nb_2O_5	120	
	Ta_2O_3	121	
	TiO_2	120,122	
RN≡C	Pt	123	124
$RHC=CH_2$	Si	37	
RC≡CH	Si(111):H	125	
$RSiX_3$ X = H, Cl, OCH_2CH_3	HfO_2	126	
	ITO	127	
	PtO	128	
	TiO_2	113,126,129	
	ZrO_2	126,129	

S-Au 25-30 Kcal/mole
Si-O 190 kcal/mole

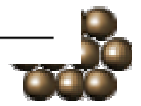

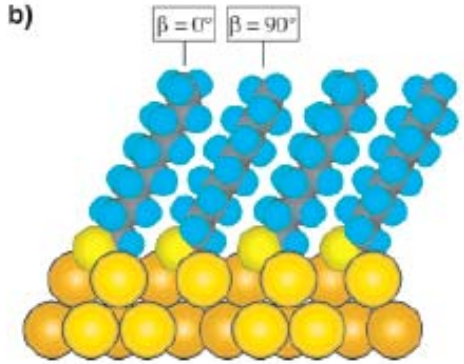

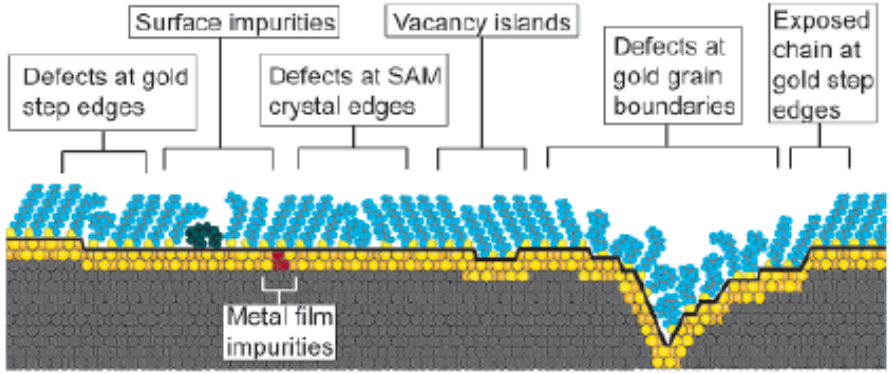

Figure 7. Schematic illustration of some of the intrinsic and extrinsic defects found in SAMs formed on polycrystalline substrates. The dark line at the metal−sulfur interface is a visual guide for the reader and indicates the changing topography of the substrate itself.

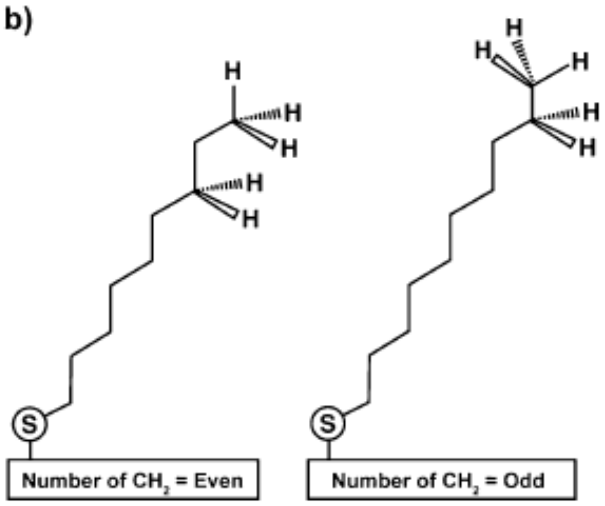

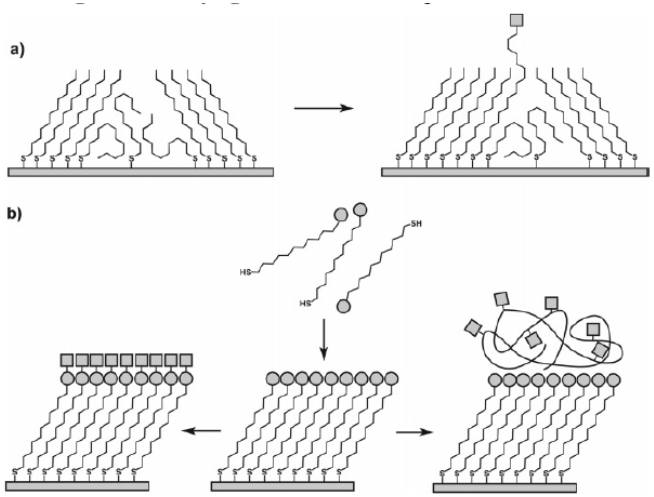

[c] (a) Insertion of a functional adsorbate at a defect site in a preformed SAM. (b) Transformation of a SAM with exposed functional groups (circles) by either chemical reaction or adsorption of another material.

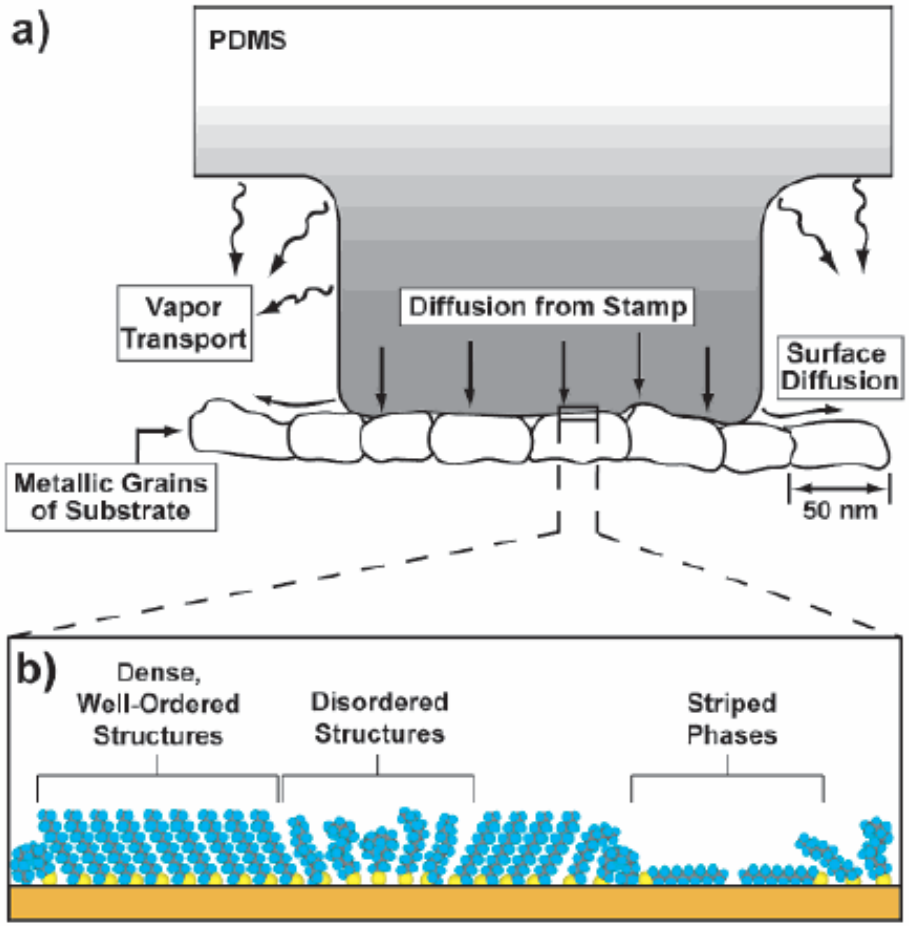

Figure 12. (a) Schematic illustration depicting the application of a PDMS stamp containing thiols to a polycrystalline metal film. The primary mechanisms of mass transport from the stamp to the surface are shown. The grayscale gradient approximates the concentration of thiols adsorbed in the stamp itself. (b) Magnified schematic view that illustrates the variety of structural arrangements found in SAMs prepared by μCP when the stamp is wetted with a 1−10 mM solution and applied to the substrate for 1−10 s.

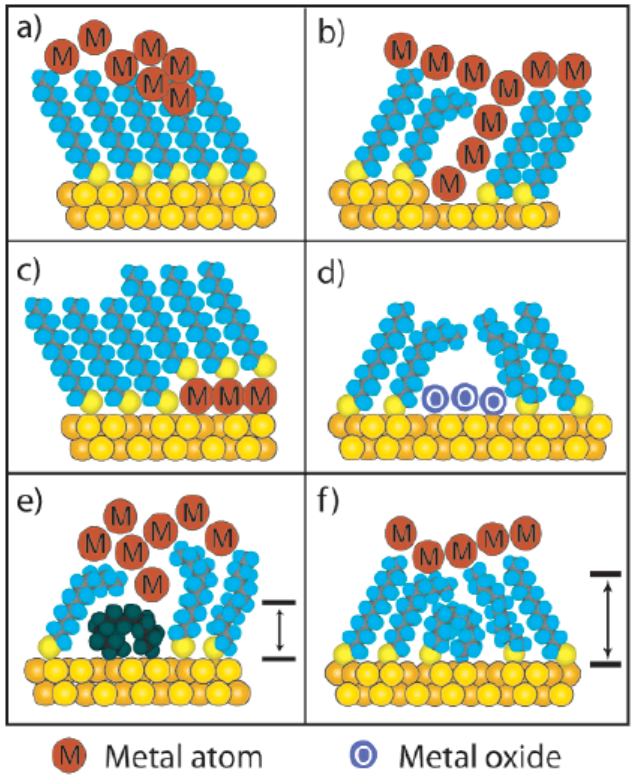

Figure 17. Schematic illustration of the types of defects in SAMs that can influence the rate of electron transfer in two-terminal (or three-terminal) devices. (a) Chemical reaction with the organic component of SAMs during evaporation of metal films. (b) Formation of metallic filaments during evaporation or operation of the device. (c) Deposition of adlayers of metal on the surface of the substrate supporting the SAM. (d) Formation of oxide impurities on the surface. (e) Organic (or organometallic) impurities in the SAM. (f) Thin regions in the SAM resulting from conformational and structural defects. In e and f the dimension normal to the surface that is denoted by the black arrows indicates the approximate shortest distance between the two metal surfaces; note that these distances are less than the nominal thickness of the ordered SAM.

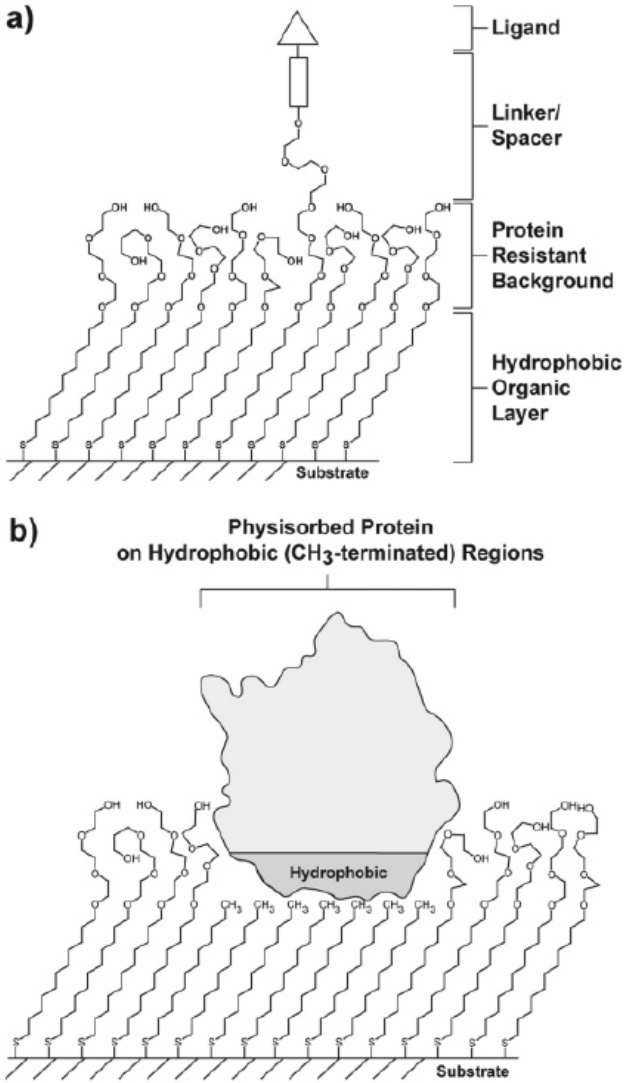

Figure 21. Schematic illustrations of (a) a mixed SAM and (b) a patterned SAM. Both types are used for applications in biology and biochemistry.

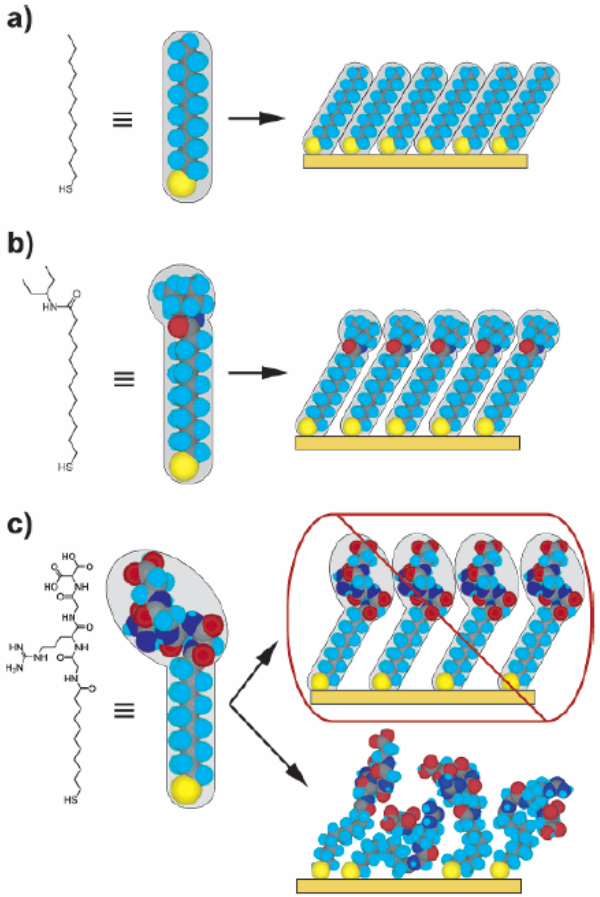

Figure 22. Schematic diagram illustrating the effects that large terminal groups have on the packing density and organization of SAMs. (a) Small terminal groups such as $-CH_3$, $-CN$, etc., do not distort the secondary organization of the organic layer and have no effect on the sulfur arrangement. (b) Slightly larger groups (like the branched amide shown here) begin to distort the organization of the organic layer, but the strongly favorable energetics of metal−sulfur binding drive a highly dense arrangement of adsorbates. (c) Large terminal groups (peptides, proteins, antibodies) sterically are unable to adopt a secondary organization similar to that for alkanethiols with small terminal groups. The resulting structures probably are more disordered and less dense than those formed with the types of molecules in a and b.

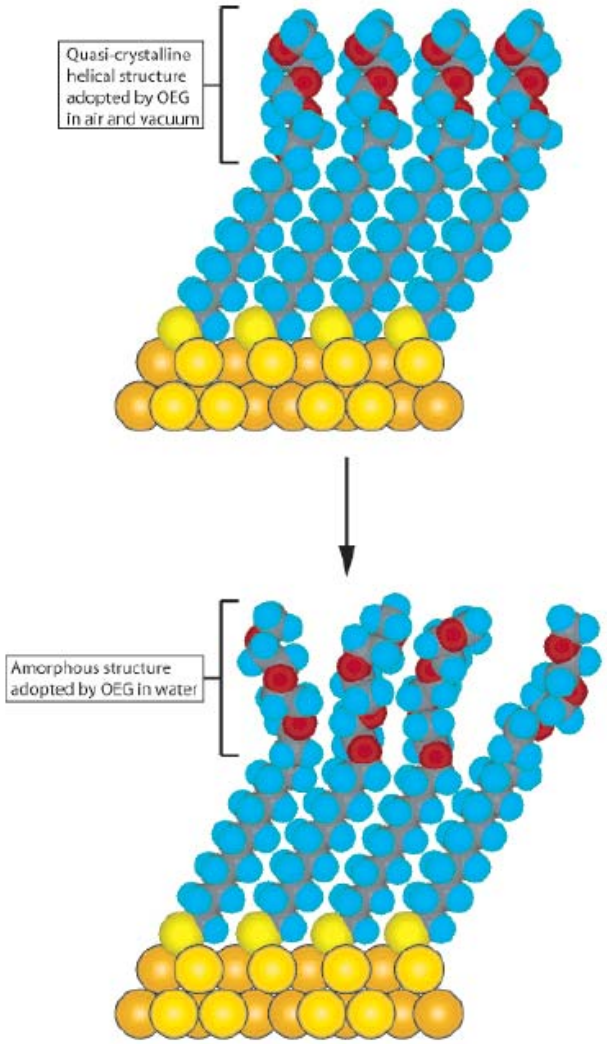

Figure 23. Schematic illustration of the order−disorder transition evidenced by SAMs of alkanethiolates terminated with triethylene glycol. The EG_3 group loses conformational ordering upon solvation in water.

Control of crystal nucleation by patterned self-assembled monolayers

NATURE | VOL 398 | 8 APRIL 1999

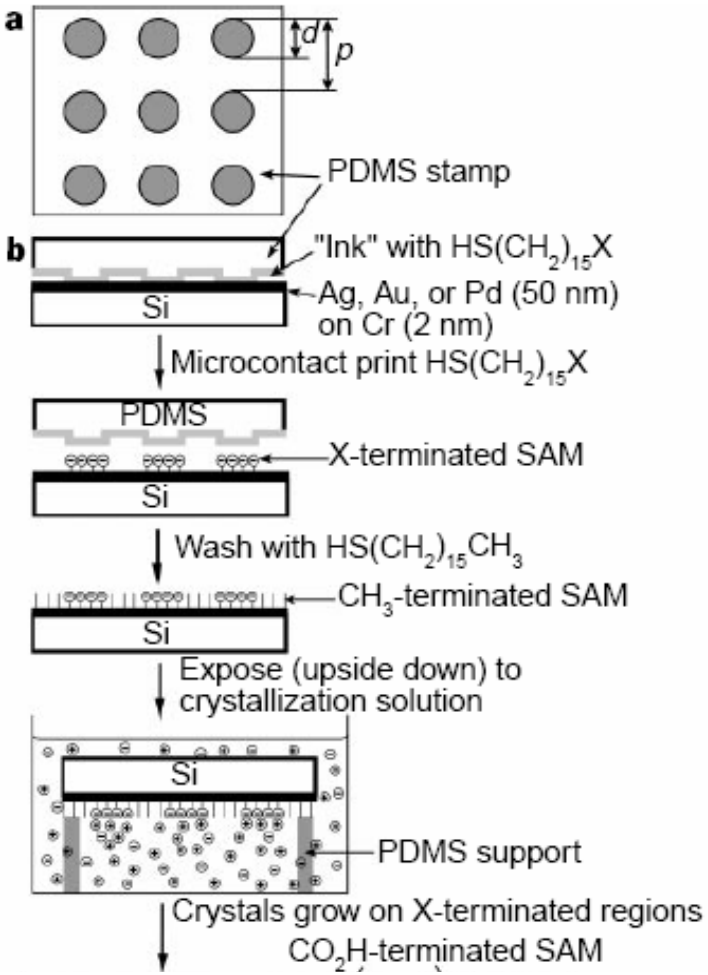

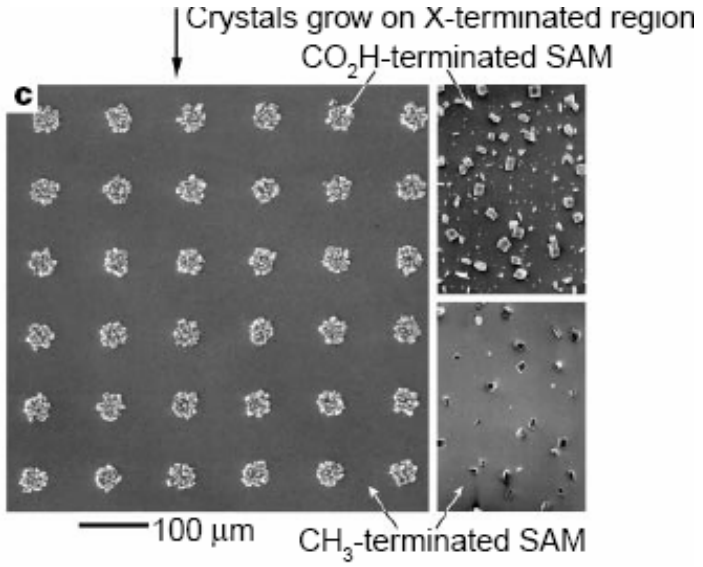

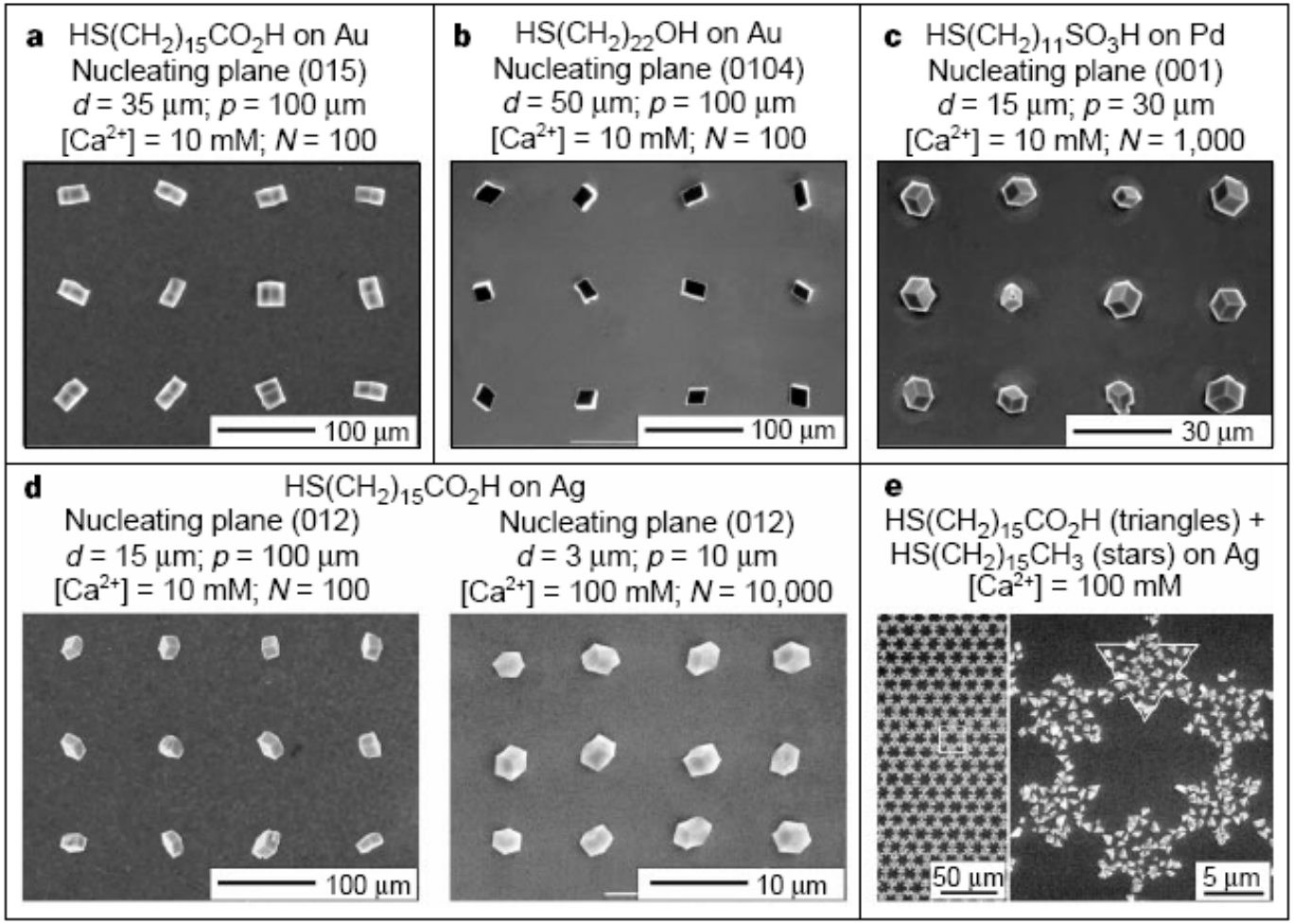
a
HS(CH2)15CO2H on Au
Nucleating plane (015)
d = 35 μm; p = 100 μm
[Ca2+] = 10 mM; N = 100
100 μm
b
HS(CH2)22OH on Au
Nucleating plane (0104)
d = 50 μm; p = 100 μm
[Ca2+] = 10 mM; N = 100
100 μm
c
HS(CH2)11SO3H on Pd
Nucleating plane (001)
d = 15 μm; p = 30 μm
[Ca2+] = 10 mM; N = 1,000
30 μm
d
HS(CH2)15CO2H on Ag
Nucleating plane (012)
d = 15 μm; p = 100 μm
[Ca2+] = 10 mM; N = 100
100 μm
Nucleating plane (012)
d = 3 μm; p = 10 μm
[Ca2+] = 100 mM; N = 10,000
10 μm
e
HS(CH2)15CO2H (triangles) +
HS(CH2)15CH3 (stars) on Ag
[Ca2+] = 100 mM
50 μm
5 μm

Patterning of organic single crystals

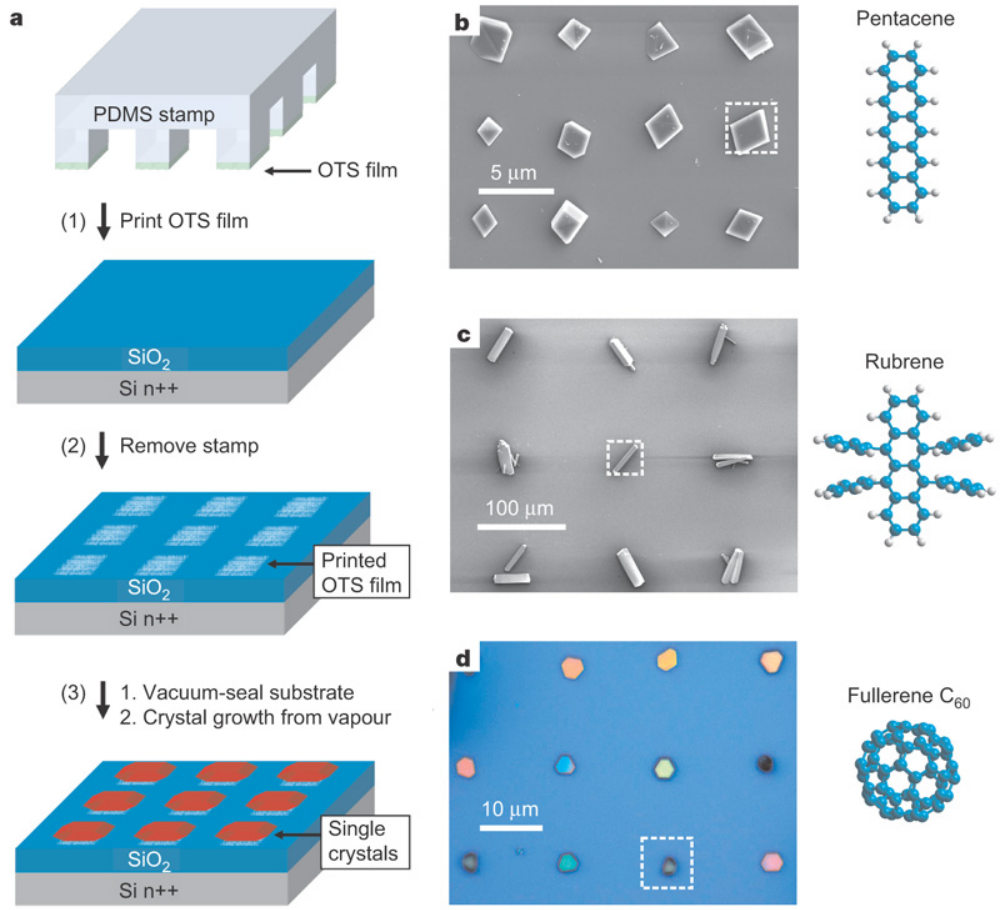

Nature 444, 913-917(14 December 2006)

Large On-Off Ratios and Negative Differential Resistance in a Molecular Electronic Device

J. Chen,[1] M. A. Reed,[1]* A. M. Rawlett,[2] J. M. Tour[2]*

19 NOVEMBER 1999 VOL 286 SCIENCE

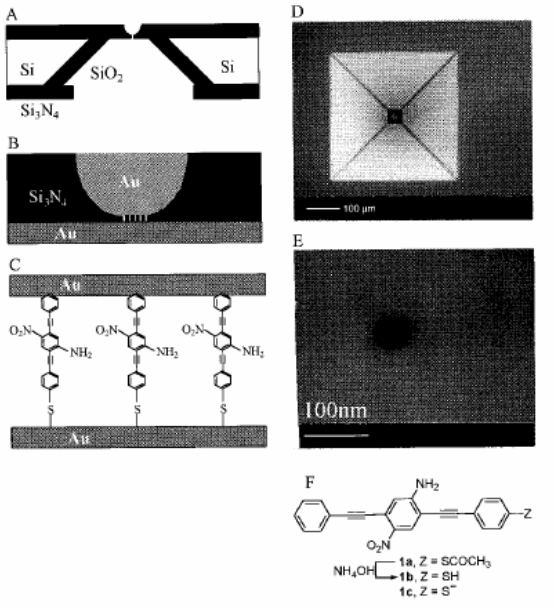

Fig. 1. Schematics of device fabrication. **(A)** Cross section of a silicon wafer with a nanopore etched through a suspended silicon nitride membrane. **(B)** Au-SAM-Au junction in the pore area. **(C)** Blowup of (B) with **1c** sandwiched in the junction. **(D)** Scanning electron micrograph (SEM) of pyramid Si structure after unisotropic Si etching [that is, the bottom view of (A)]. **(E)** SEM of an etched nanopore through the silicon nitride membrane. **(F)** The active molecular compound **1c** and its precursors the free thiol **1b** and the thiol-protected system **1a**.

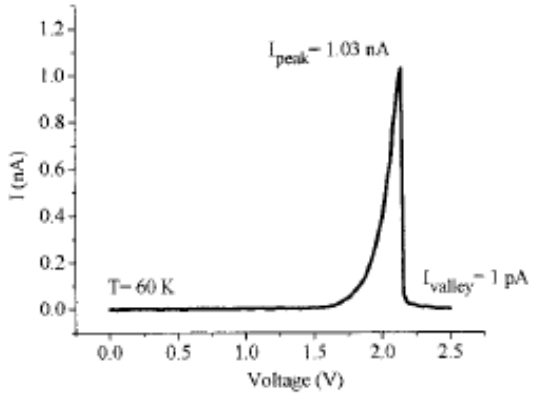

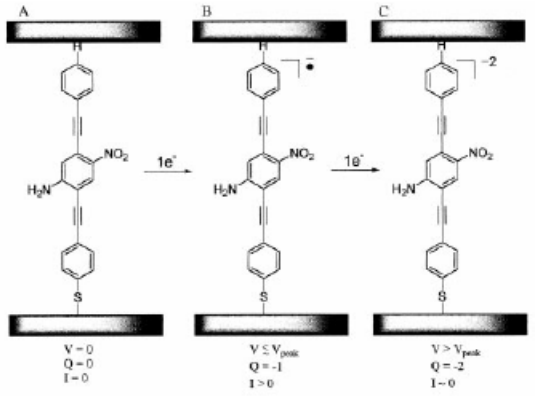

Fig. 4. Potential mechanism for the NDR effect. As voltage is applied, the molecules in the SAM (**A**) undergo a one-electron reduction to form the radical anion (**B**) that provides a conductive state. Further increase of the voltage causes another one-electron reduction to form the dianion insulating state (**C**). Q is the charge.

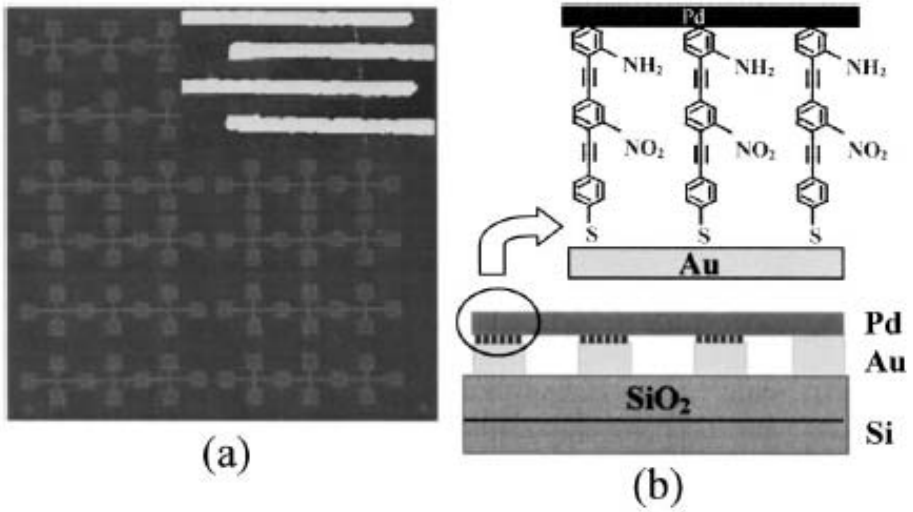

FIG. 1. (a) Optical micrograph of the nanoelectrode array. Inset: AFM image of four Au nanoelectrodes with a Pd nanowire lying across. (b) Schematic diagram of the Pd/molecular wires/Au junctions on a Si/SiO_2 substrate.

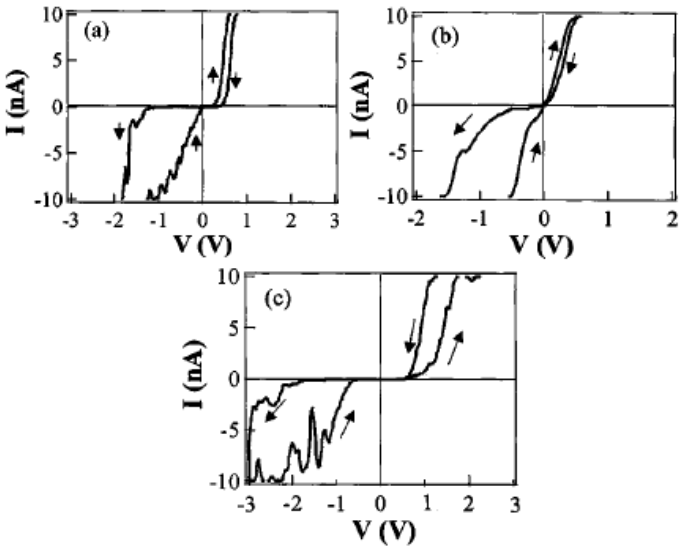

FIG. 3. Typical $I-V$ curves of molecular devices. (a), (b), and (c) correspond to molecules **a**, **b**, and **c** shown in Fig. 2, respectively.

Geometric Control of Cell Life and Death

SCIENCE • VOL. 276 • 30 MAY 1997

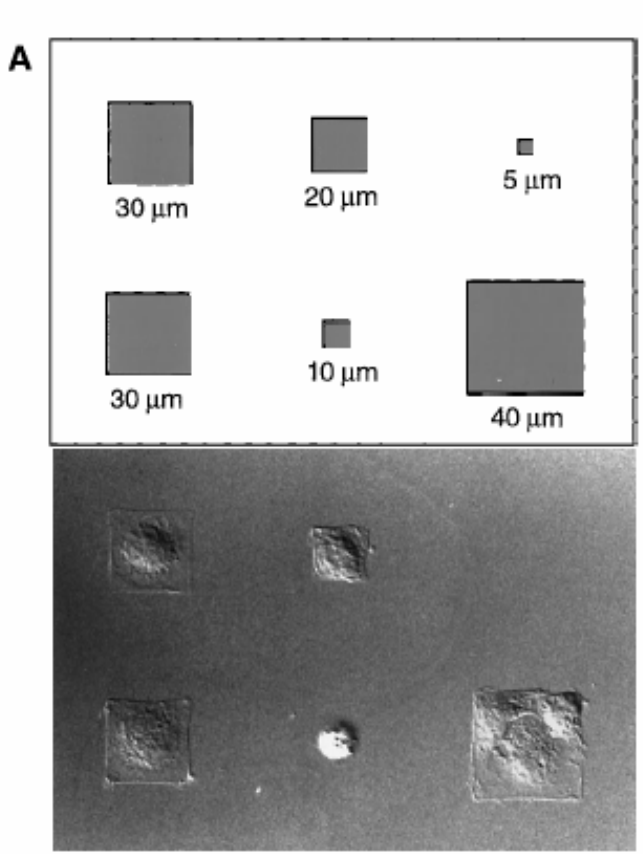

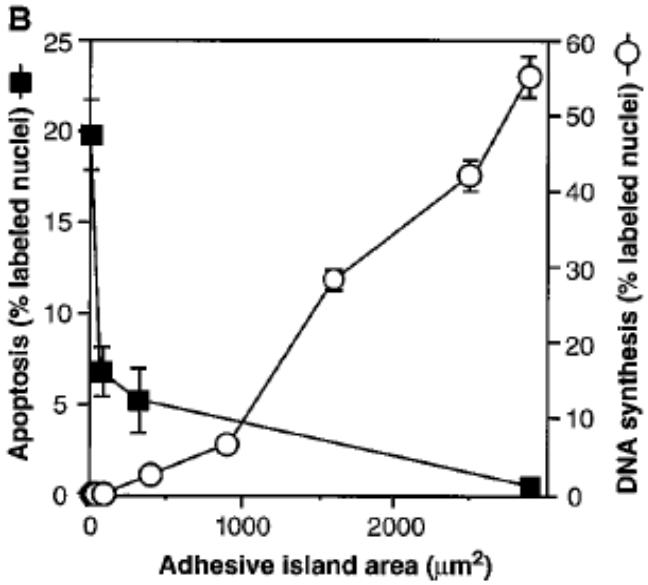

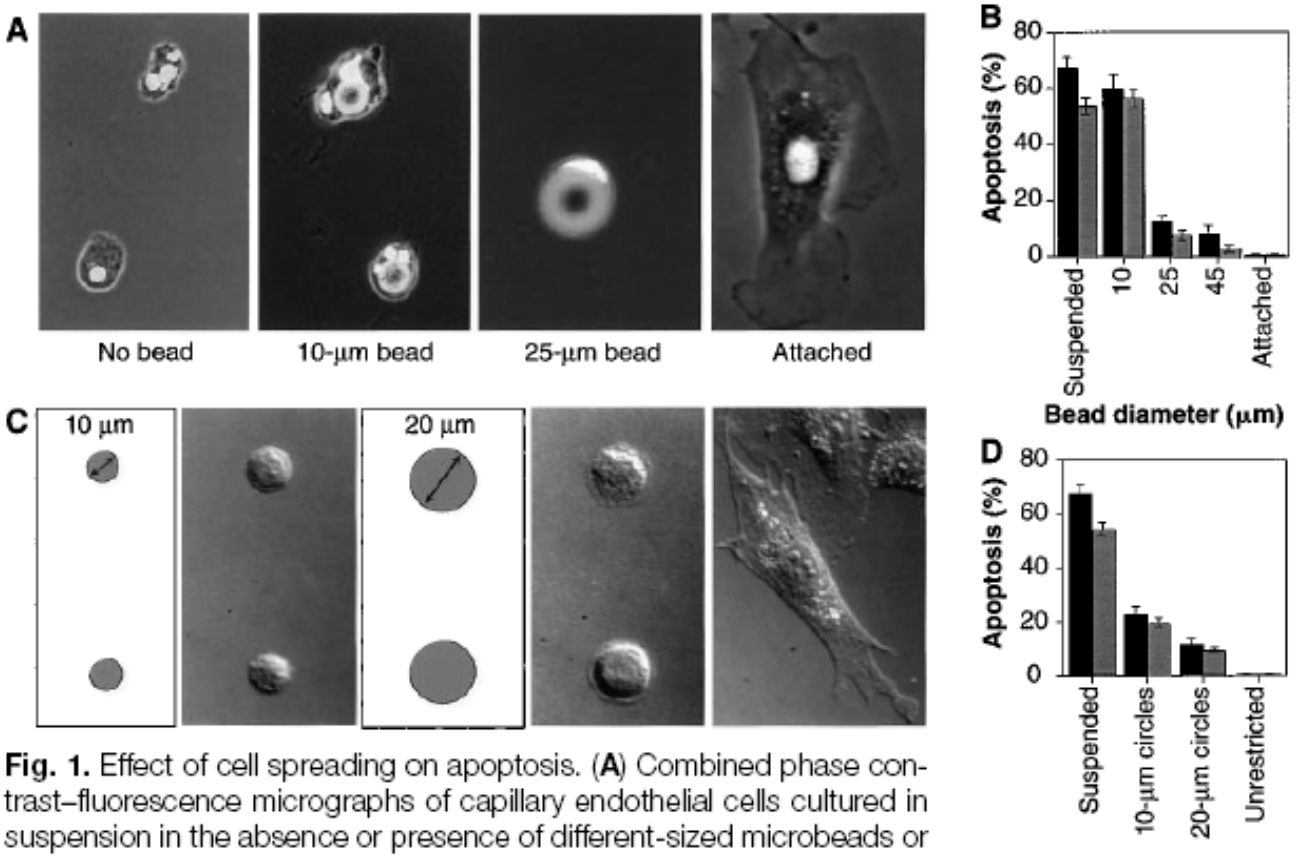

Fig. 1. Effect of cell spreading on apoptosis. (**A**) Combined phase contrast–fluorescence micrographs of capillary endothelial cells cultured in suspension in the absence or presence of different-sized microbeads or attached to a planar culture dish coated with FN for 24 hours (*28*). In the highly spread cell on the 25-μm bead, only the flattened 4′,6′-diamidino-2-phenylindole (DAPI)–stained nucleus is clearly visible. (**B**) Apoptosis in cells attached to different-sized beads, in suspension, or attached to a dish. The apoptotic index was quantitated by measuring the percentage of cells exhibiting positive TUNEL staining (black bars) (Boehringer Mannheim), which detects DNA fragmentation; similar results were obtained by analyzing changes in nuclear condensation and fragmentation in cells stained with DAPI at 24 hours (gray bars). Apoptotic indices were determined only within single cells bound to single beads. Error bars indicate SEM. (**C**) Differential interference-contrast micrographs of cells plated on substrates micropatterned with 10- or 20-μm-diameter circles coated with FN (left), by a microcontact printing method (*29*) or on a similarly coated unpatterned substrate (right). (**D**) Apoptotic index of cells attached to different-sized adhesive islands coated with a constant density of FN for 24 hours; similar results were obtained with human and bovine capillary endothelial cells (*28*). Bars same as in (B).

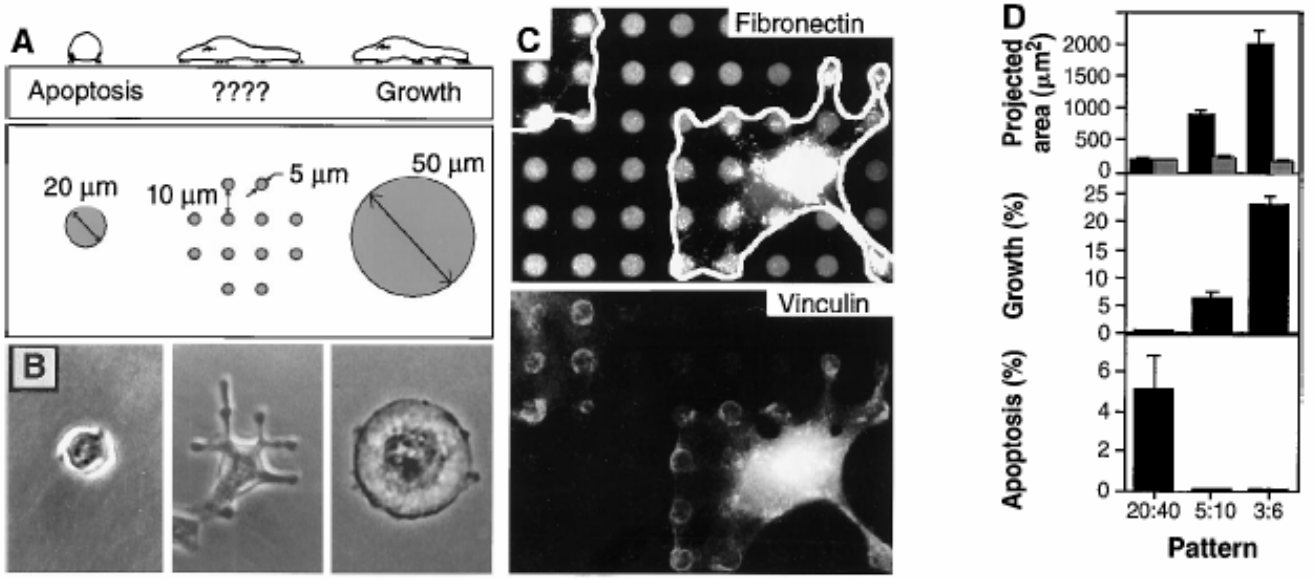

Fig. 3. Cell-ECM contact area versus cell spreading as a regulator of cell fate. (**A**) Diagram of substrates used to vary cell shape independently of the cell-ECM contact area. Substrates were patterned with small, closely spaced circular islands (center) so that cell spreading could be promoted as in cells on larger, single round islands, but the ECM contact area would be low as in cells on the small islands. (**B**) Phase-contrast micrographs of cells spread on single 20- or 50-μm-diameter circles or multiple 5-μm circles patterned as shown in (A). (**C**) Immunofluorescence micrographs of cells on a micropatterned substrate stained for FN (top) and vinculin (bottom). White outline indicates cell borders; note circular rings of vinculin staining, which coincide precisely with edges of the FN-coated adhesive islands. (**D**) Plots of projected cell area (black bars) and total ECM contact area (gray bars) per cell (top), growth index (middle), and apoptotic index (bottom) when cells were cultured on single 20-μm circles or on multiple circles 5 or 3 μm in diameter separated by 40, 10, and 6 μm, respectively.

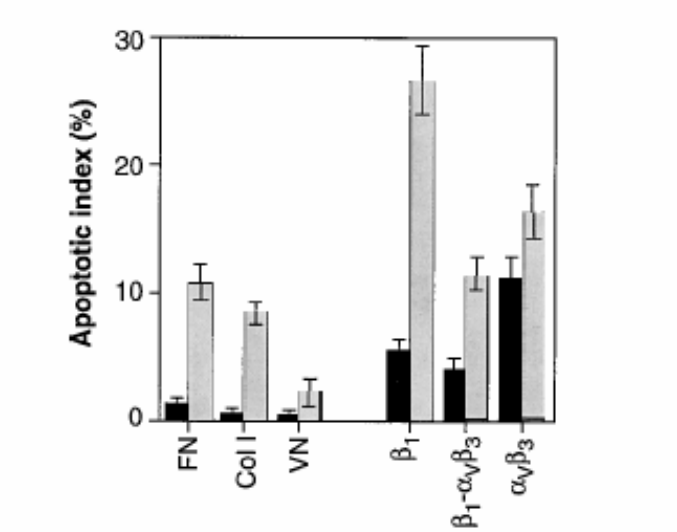

Fig. 4. Role of different integrin ligands in cell shape–regulated apoptosis. Apoptotic indices (percentage positive TUNEL staining) for cells cultured for 24 hours on unpatterned substrates (black bars) or on 20-μm circles (gray bars) coated with FN, type I collagen (Col I), vitronectin (VN), anti-β_1, anti-$\alpha_V\beta_3$, or antibodies to both integrin β_1 and integrin $\alpha_V\beta_3$ (*29*).

hexadecanethiol [$HS(CH_2)_{15}CH_3$] was printed onto gold-coated substrates with a flexible stamp containing a relief of the desired pattern. The substrate was immersed immediately in 2 mM tri(ethylene glycol)-terminated alkanethiol [$HS(CH_2)_{11}(OCH_2CH_2)_3OH$ in ethanol], which coated the remaining bare regions of gold. When these substrates were immersed in a solution of FN, vitronectin, or type I collagen (50 μg/ml in phos-

Electrochemical Desorption of Self-Assembled Monolayers Noninvasively Releases Patterned Cells from Geometrical Confinements

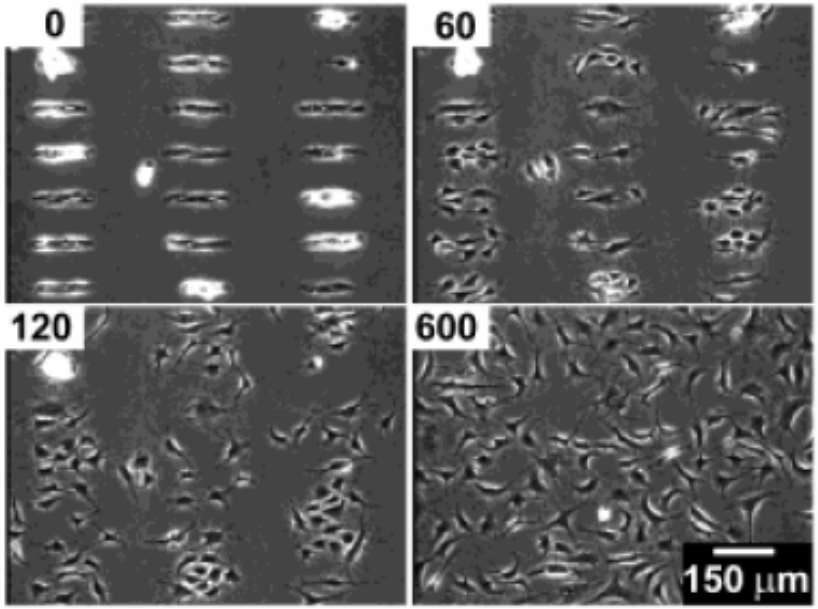

Figure 1. BCE cells were allowed to attach to a surface patterned with $C_{11}EG_3$ and C_{18}. Application of a cathodic voltage pulse (−1.2 V for 30 s in this case) released the cells from the microislands. The numbers indicate the time elapsed (in minutes) after the voltage pulse.

■ **J. AM. CHEM. SOC. 2003**, *125*, 2366−2367

Directing cell migration with asymmetric micropatterns

http://www.pnas.org/cgi/reprint/102/4/9

PNAS | January 25, 2005 | vol. 102 | no. 4 | 975

Xingyu Jiang*, Derek A. Bruzewicz*, Amy P. Wong*, Matthieu Piel†, and George M. Whitesides*‡

*Department of Chemistry and Chemical Biology, Harvard University, 12 Oxford Street, Cambridge, MA 02138; and †Department of Molecular and Cellu Biology, Harvard University, 16 Divinity Avenue, Cambridge, MA 02138

Contributed by George M. Whitesides, December 2, 2004

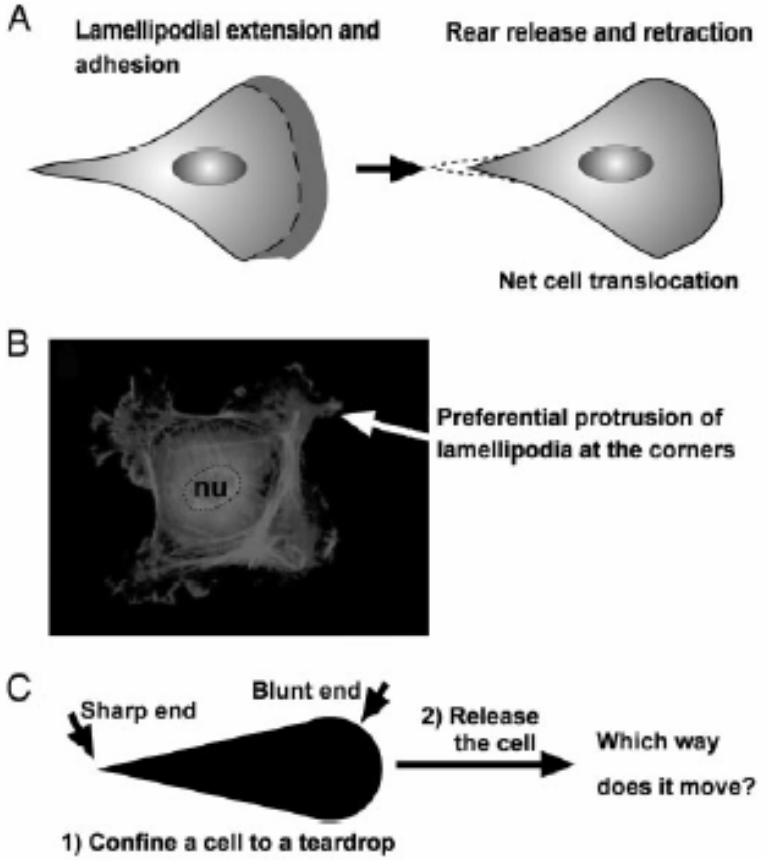

Fig. 1. A problem on cell motility. (*A*) A cartoon illustration of the migration of a typical mammalian cell on a flat surface. This teardrop shape is found in many types of cells. (*B*) Cells confined to squares preferentially extend their lamellipodia from the corners. nu, nucleus. (*C*) If a cell is confined to a shape of teardrop, will the cell preferentially extend its lamellipodia from the sharp end or from the blunt end? If released from confinement, in which direction will it likely move?

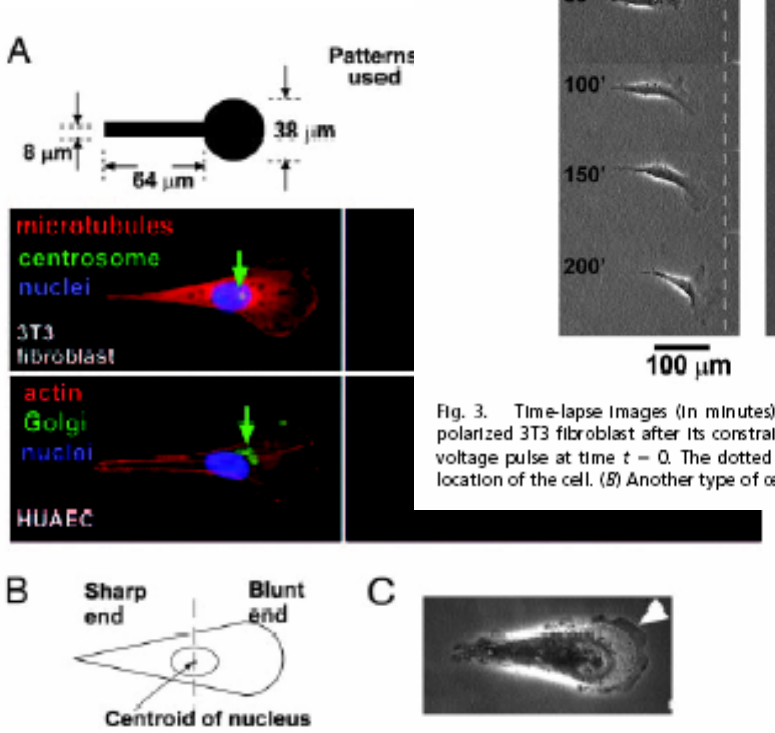

Fig. 2. Asymmetric patterns polarize immobilized cells. (*A*) The Golgi and the centrosome are located closer to the half of a cell with the blunt end. We used phallodin, antigolgin, DAPI, antitubulin, and antipericentrin to identify actin (red), the Golgi (green), the nucleus (blue), microtubules (red), and the centrosome (green), respectively. The green arrows indicate the location of centrosomes in 3T3 cells and Golgi in human umbilical artery endothelial cells (HUAEC). (*B*) We divided the cell into a half with the sharp end and a half with the blunt end by a vertical line drawn at the centroid of the nucleus; >80% ($n = 30$) of the centrosomes and Golgi were localized in the region of the wide end. (*C*) The lamellipodia of immobilized 3T3 cells tended to extend more from the blunt end as well (arrowhead). The dotted line indicates the edges of the adhesive pattern.

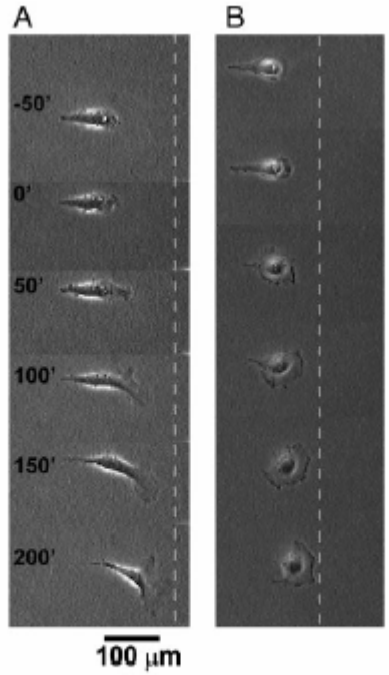

Fig. 3. Time-lapse images (in minutes) show the motility of an initially polarized 3T3 fibroblast after its constraint is released. (*A*) We applied the voltage pulse at time $t = 0$. The dotted line serves as a reference for the location of the cell. (*B*) Another type of cell, COS-7, shows similar behavior.

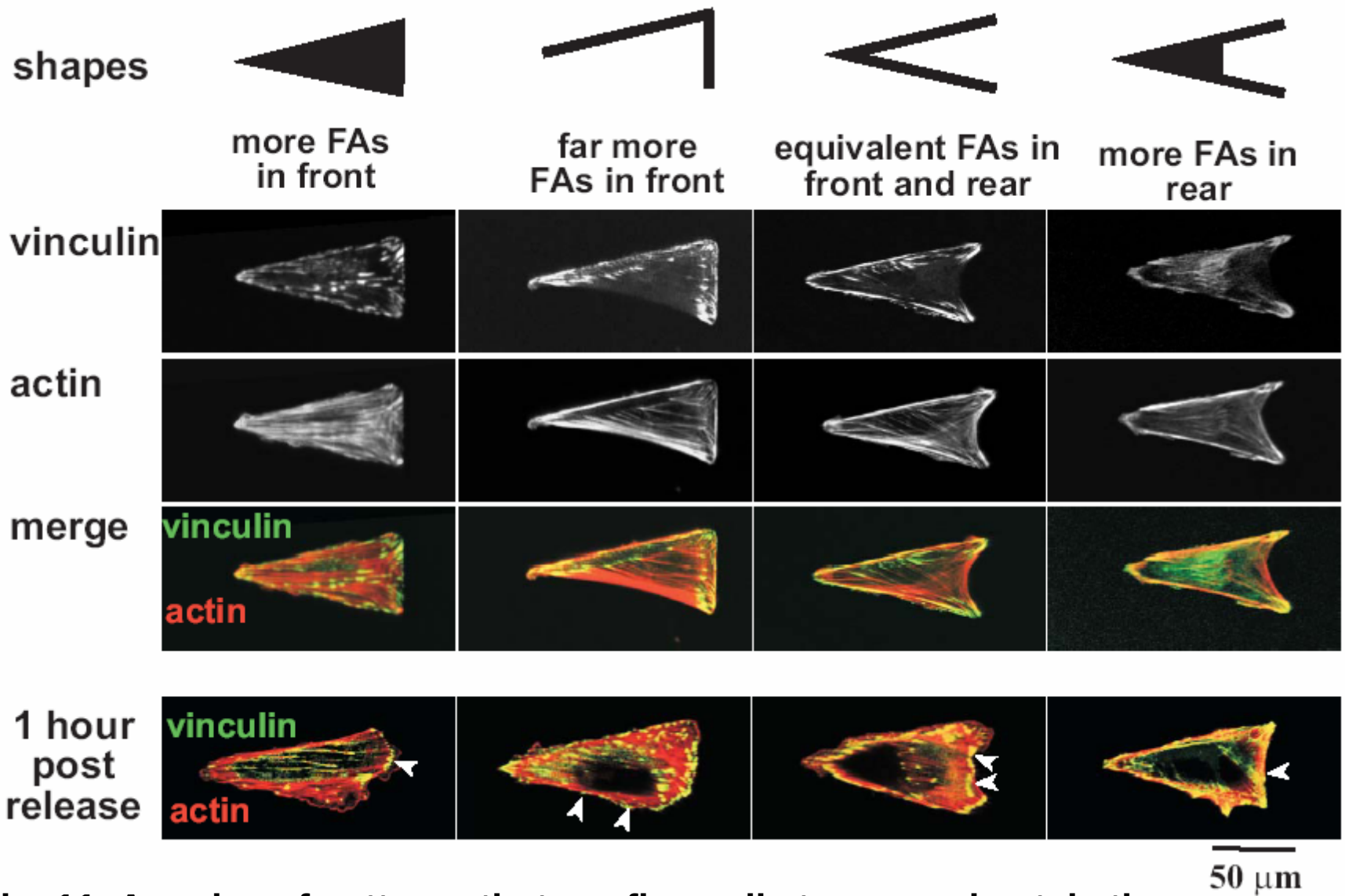

Fig. 11. A series of patterns that confine cells to approximately the same projected geometry (visualized by the actin cytoskeleton) but distribute the focal adhesions (FAs; visualized by immunostaining for vinculin) differently. The bottom row shows that new focal adhesions formed 1 h after release in areas that were inert to attachment of cells prior to release (arrowheads).

Soft-Lithography

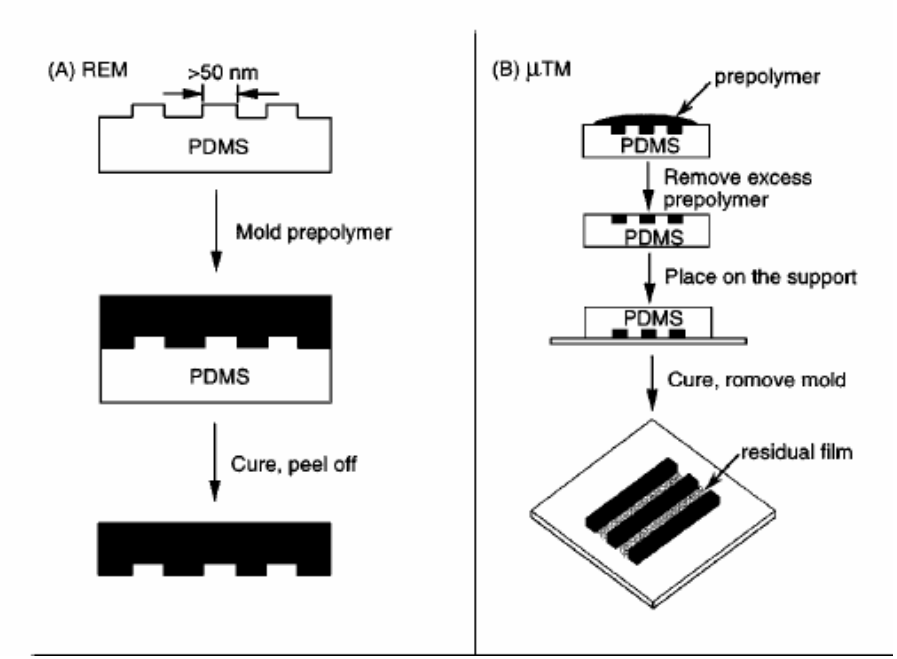

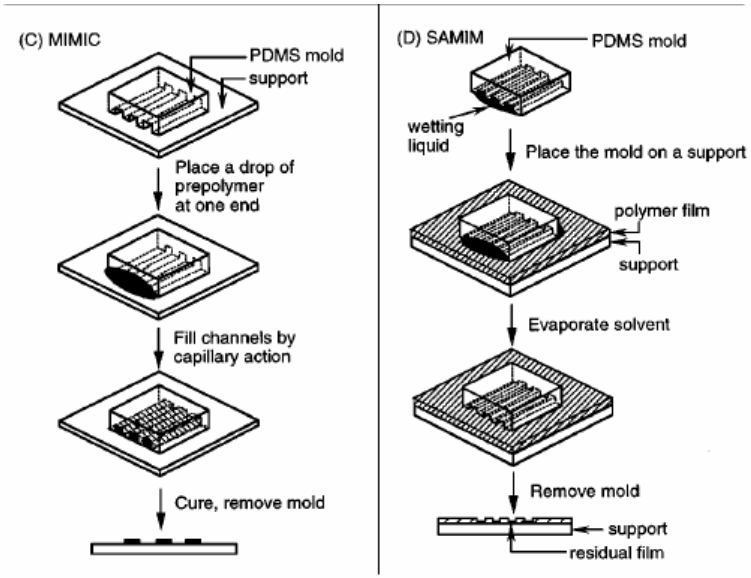

Figure 5 Schematic illustration of procedures for (*a*) replica molding (REM), (*b*) microtransfer molding (μTM), (*c*) micromolding in capillaries (MIMIC), and (*d*) solvent-assisted micromolding (SAMIM).

Electrophoresis 2002, 23, 3461–3473

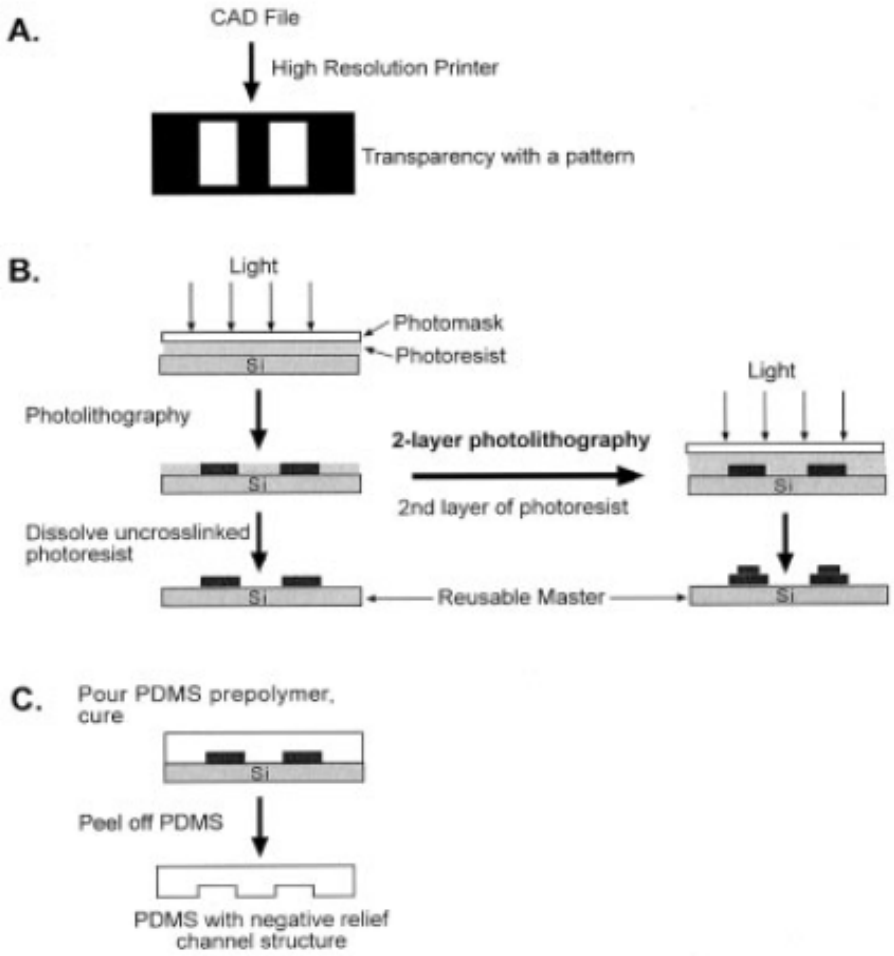

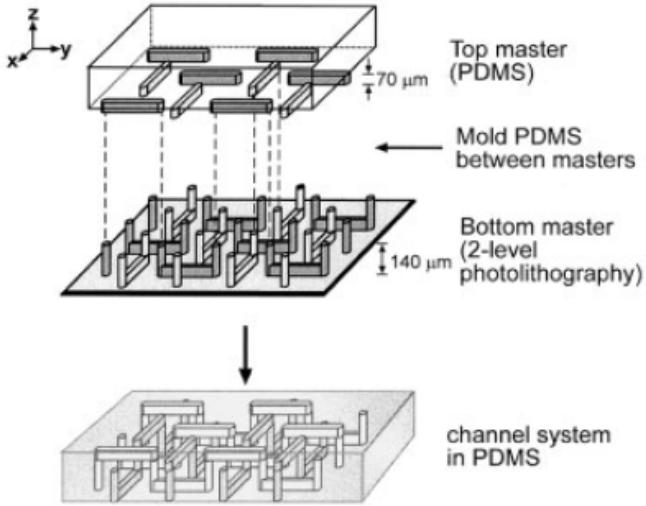

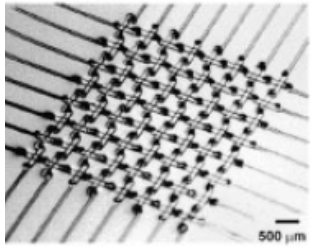

D.

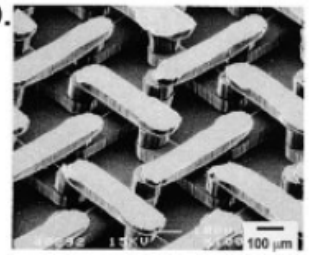

Replication Result

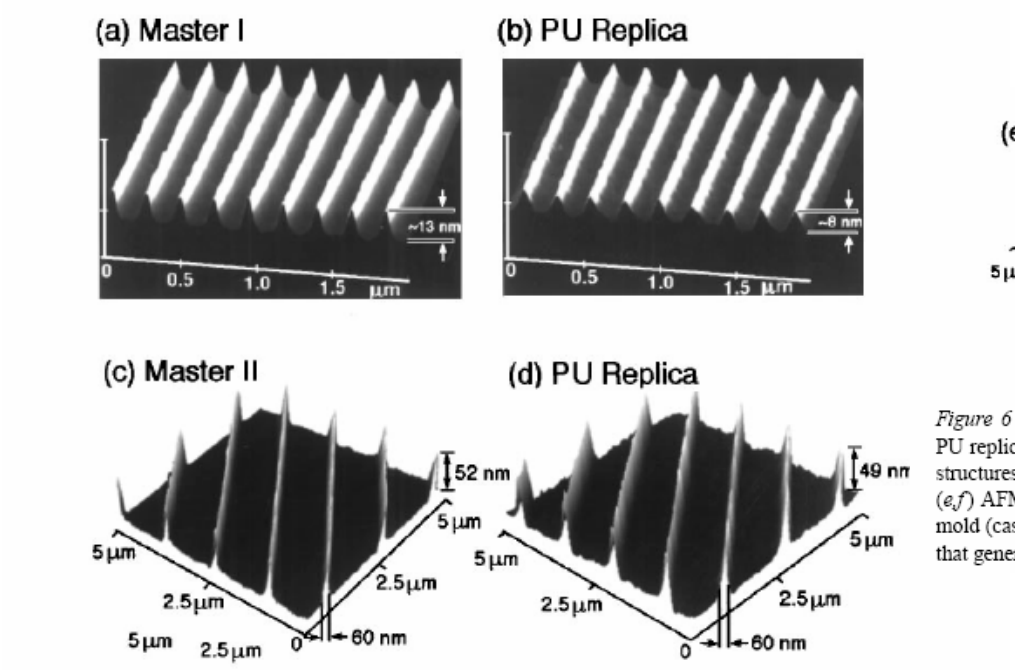

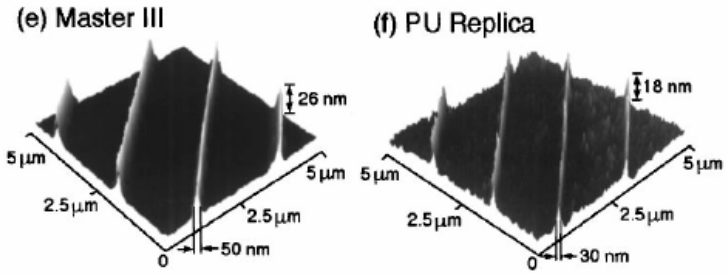

Figure 6 (*a,b*) Atomic force microscopy (AFM) images of Cr structures on a master, and a PU replica prepared from a PDMS mold cast from this master (153). (*c,d*) AFM images of Au structures on another master, and a PU replica produced from a PDMS mold cast from this master. (*e,f*) AFM images of Au structures on a third master, and a PU replica fabricated from a PDMS mold (cast from this master) while this mold was mechanically deformed by bending in a manner that generated narrower lines.

Nanosphere Lithography

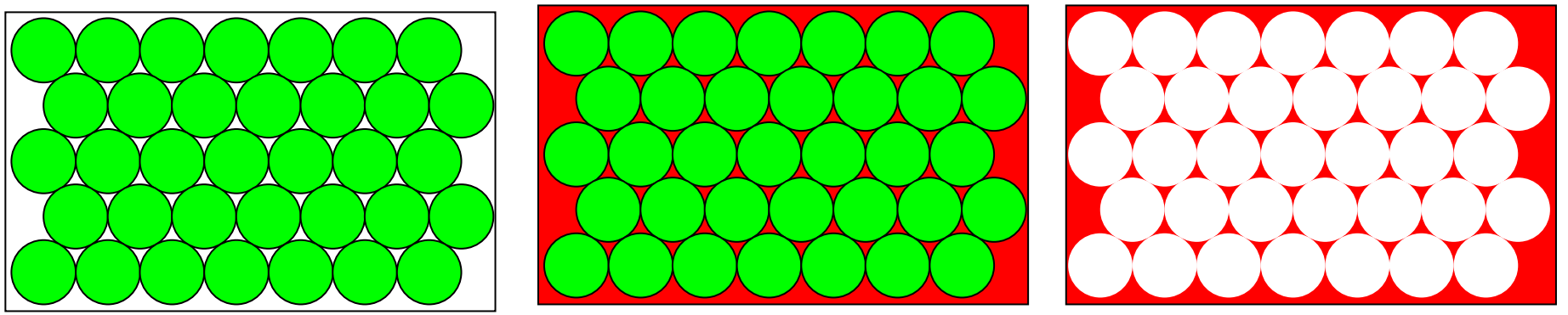

Single layer → Metal deposition → Lift-off

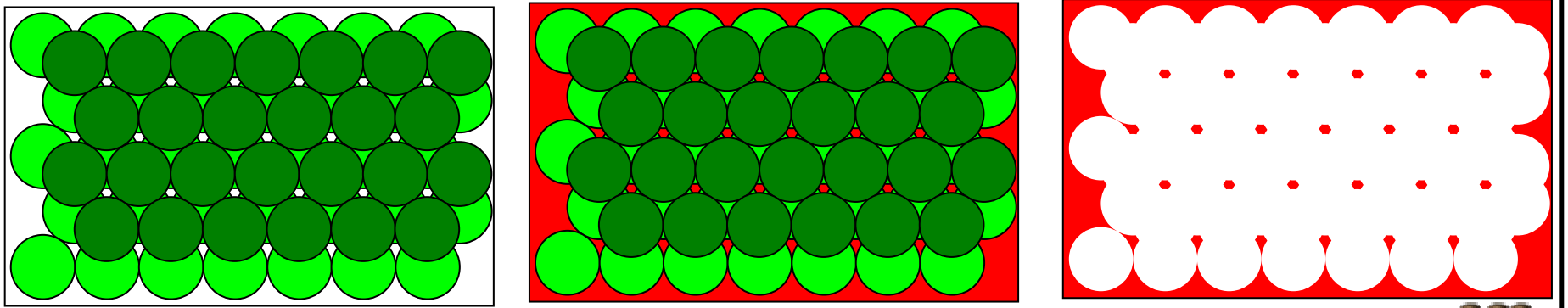

Double layer Metal deposition Lift-off

Array Dimension

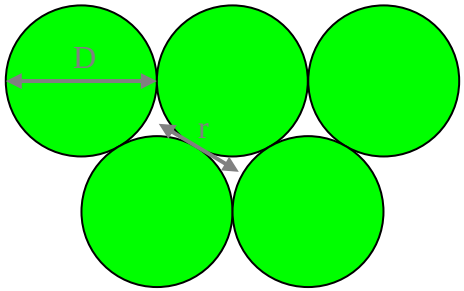

$$r = \frac{1}{\sqrt{3}} D$$

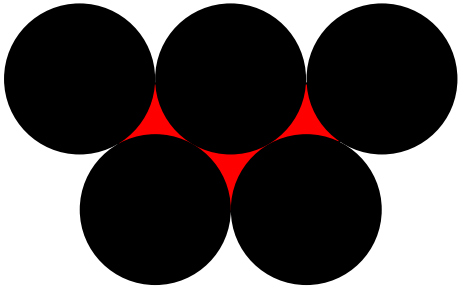

$$a = \frac{3}{2}\left(\sqrt{3} - 1 - \frac{1}{\sqrt{3}}\right) D$$

~1/4 D

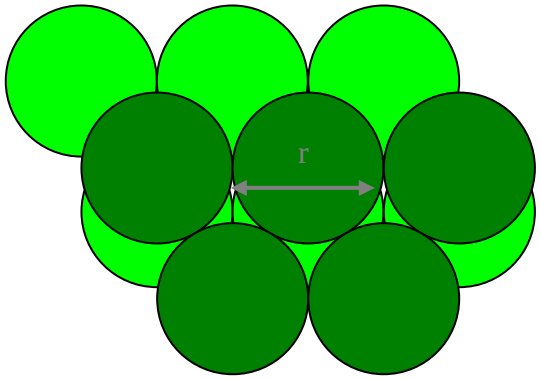

$$r = D$$

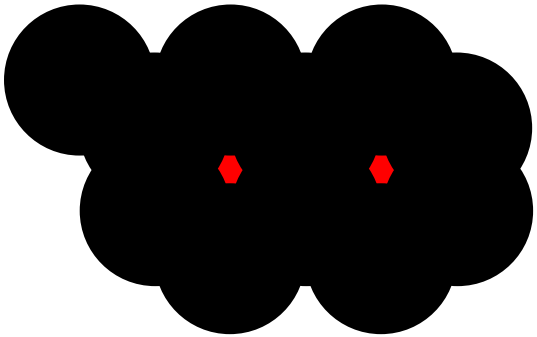

$$a = \left(\sqrt{3} - 1 - \frac{1}{\sqrt{3}}\right) D$$

~1/7 D

Optical Image of PS Template

800 nm PS

Nanosphere Lithography

350 nm

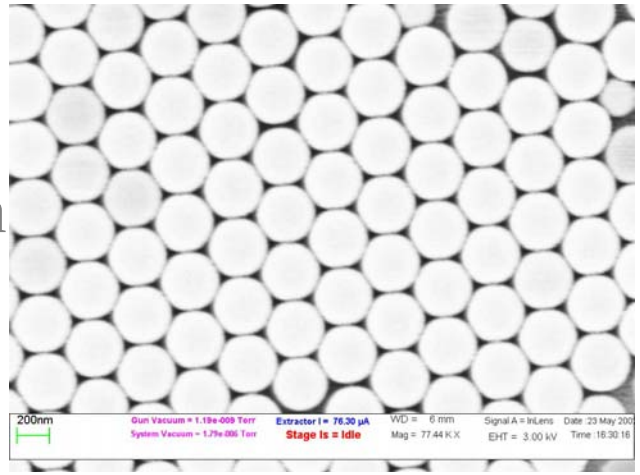

550 nm

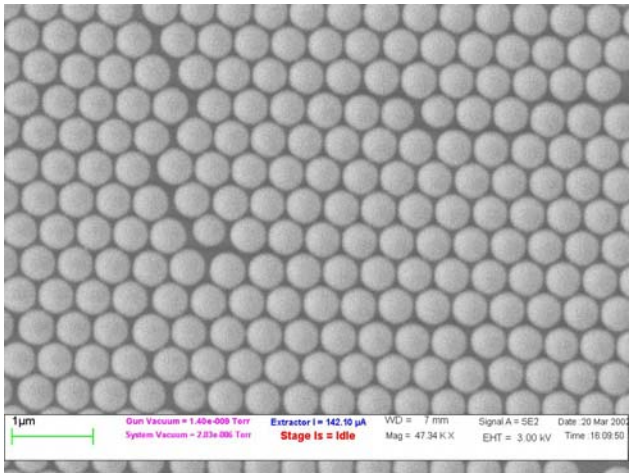

400 nm

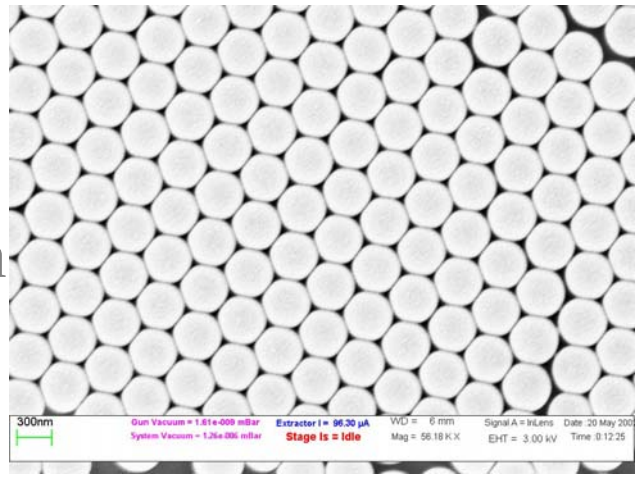

880 nm

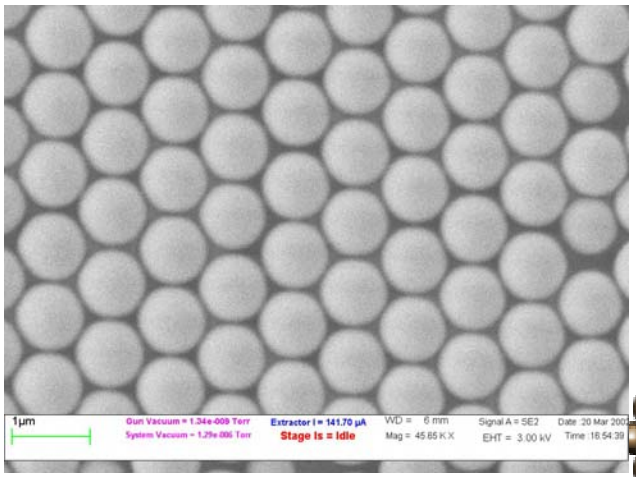

Single Layer Templates

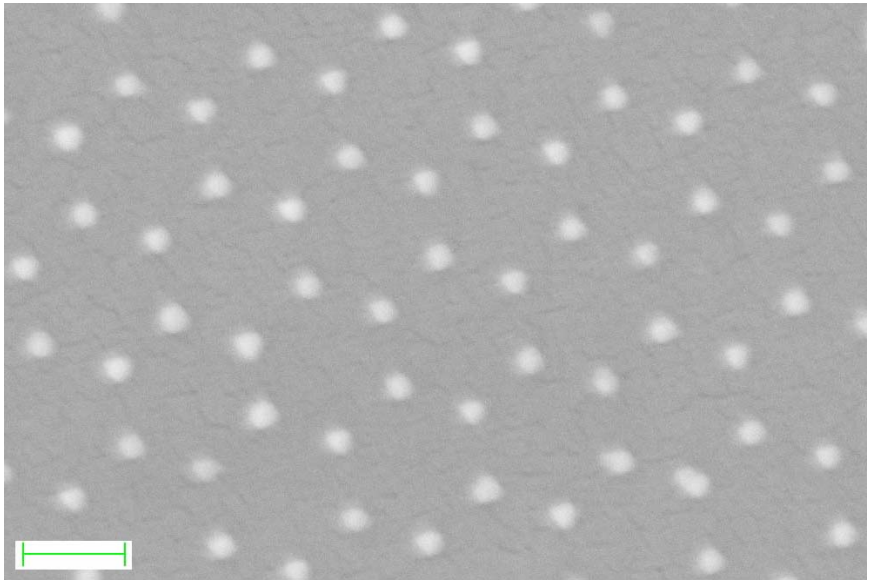

280 nm

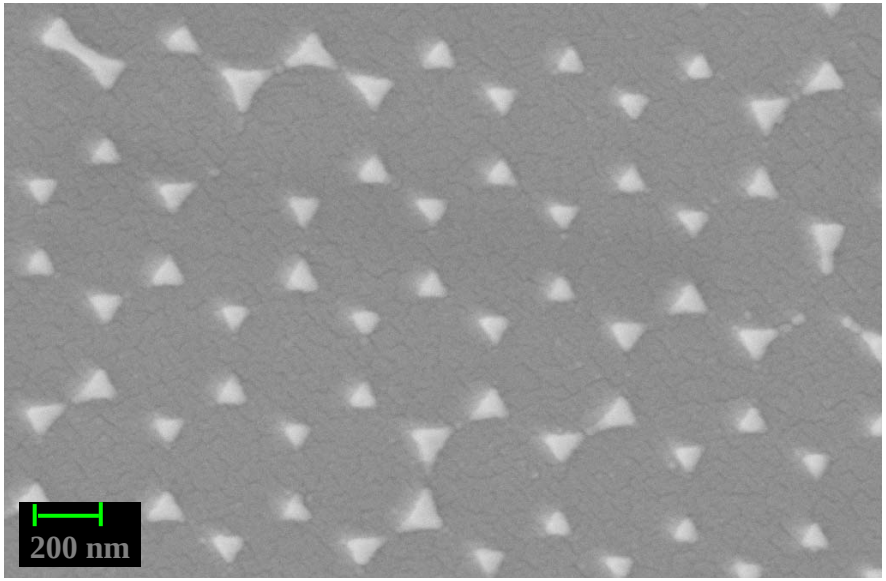

550 nm

Double Layer Templates

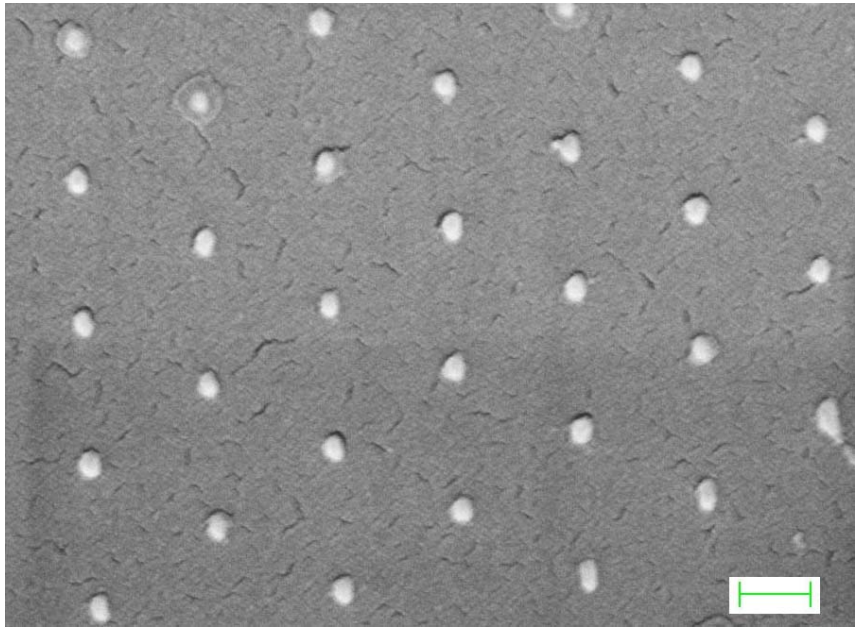

400 nm

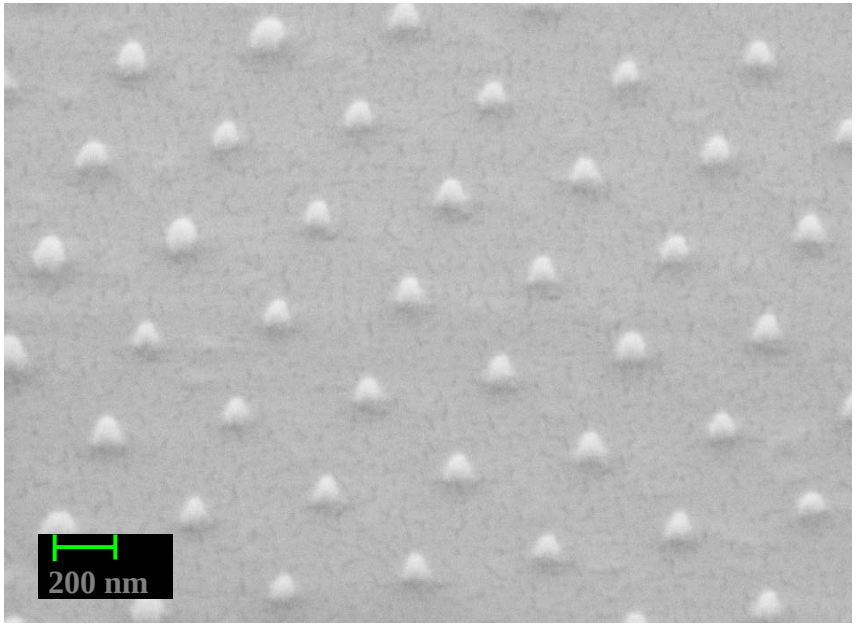

550 nm

Ordered Metal Nanohole Arrays Made by a Two-Step Replication of Honeycomb Structures of Anodic Alumina

Hideki Masuda* and Kenji Fukuda

SCIENCE • VOL. 268 • 9 JUNE 1995

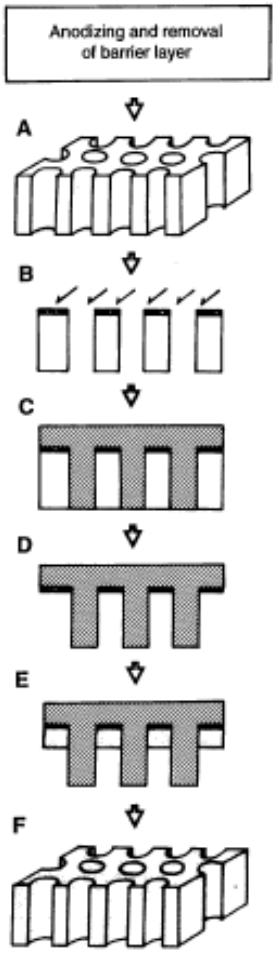

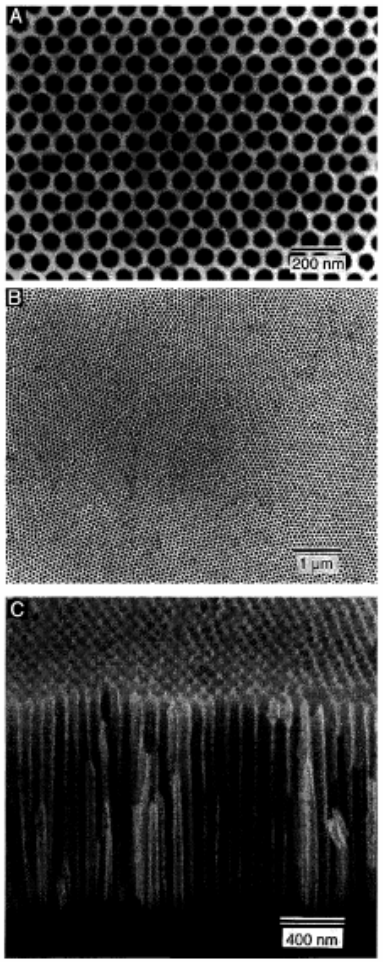

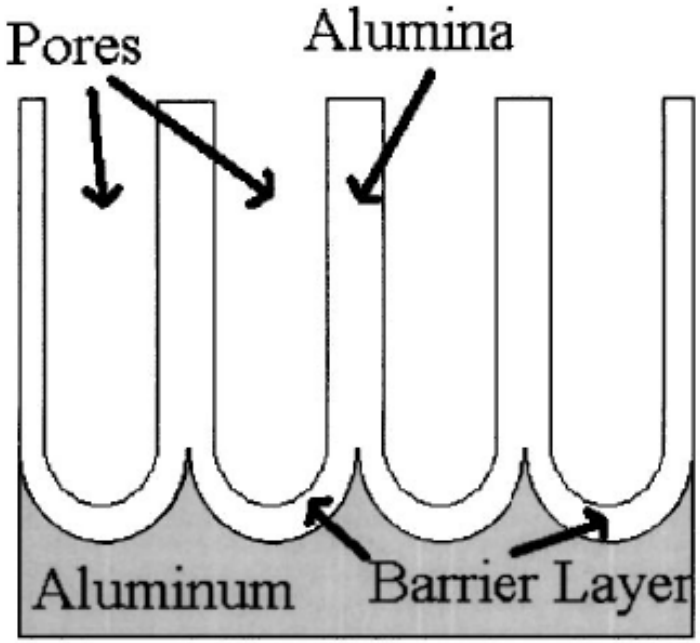

FIG. 1. Diagram of the typical porous alumina structure when fabricated using bulk aluminum.

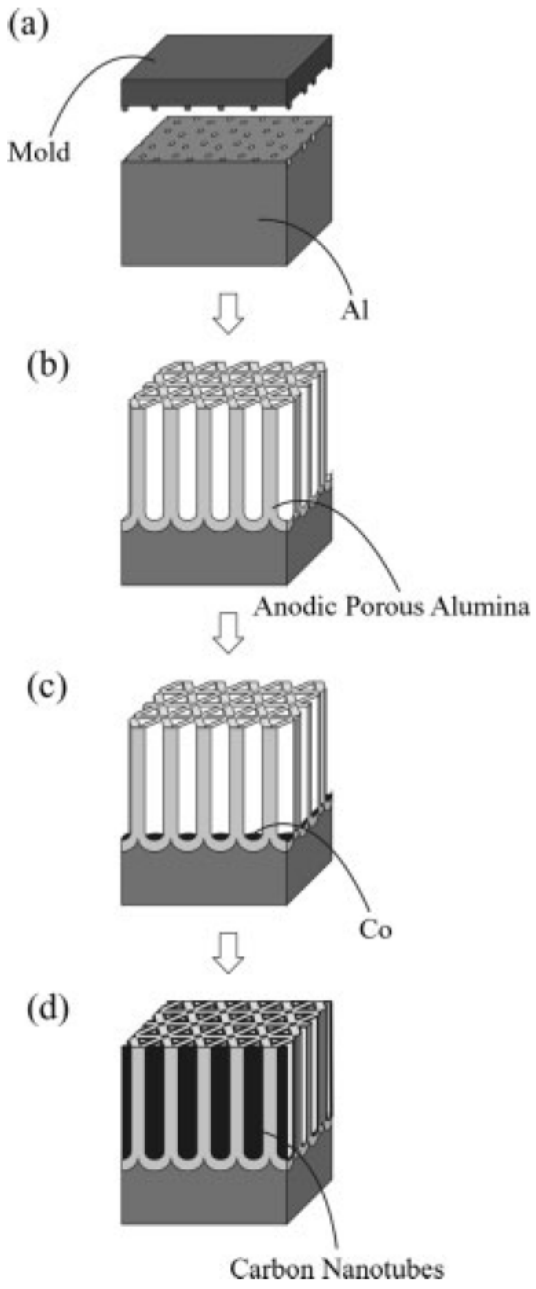
(a)
Mold
Al
(b)
Anodic Porous Alumina
(c)
Co
(d)
Carbon Nanotubes

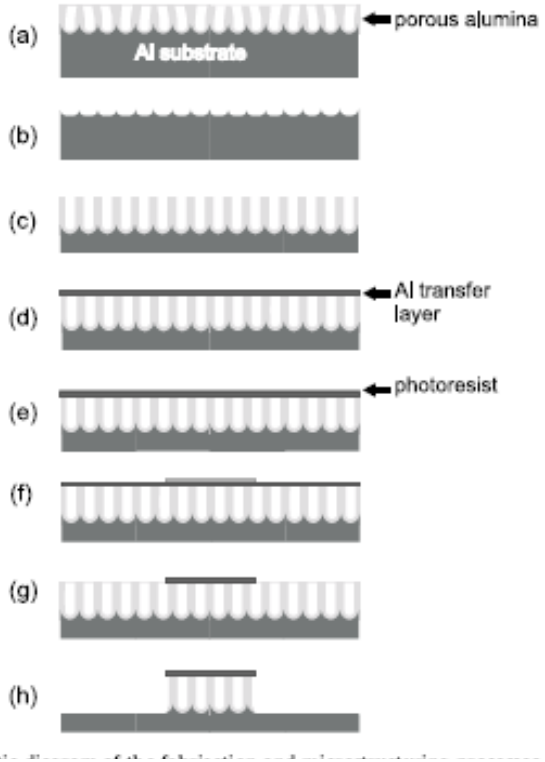
(a)
porous alumina
Al substrate
(b)
(c)
(d)
Al transfer layer
(e)
photoresist
(f)
(g)
(h)

Project IV: Growth of 1D Nanofibers Using AAO Templates

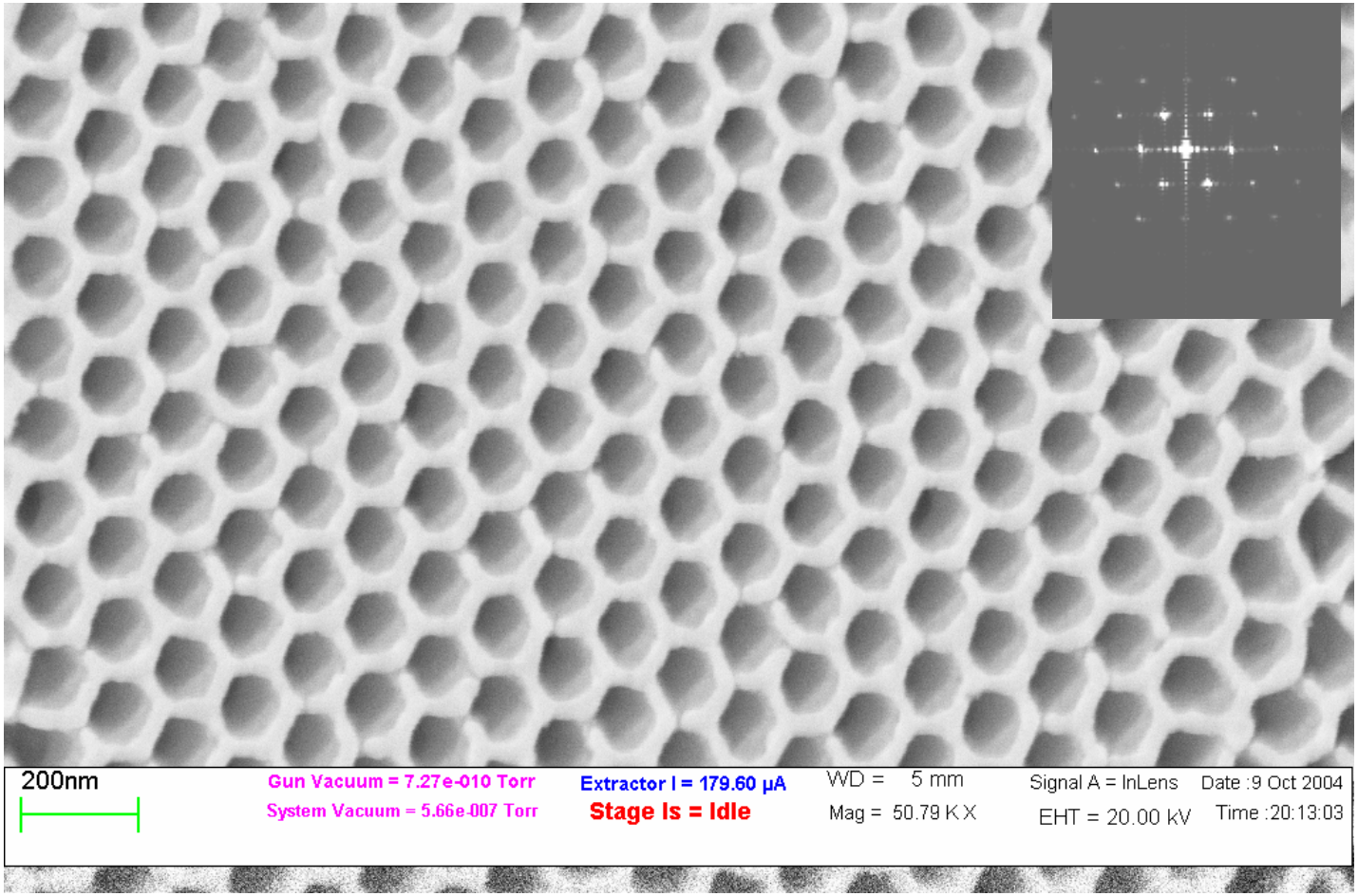

AAO Templates

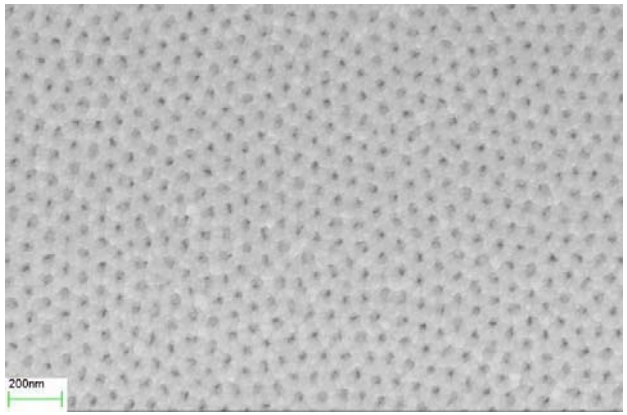

30 V

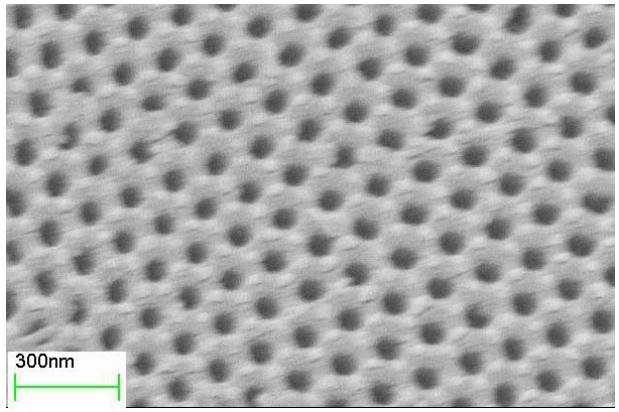

50 V

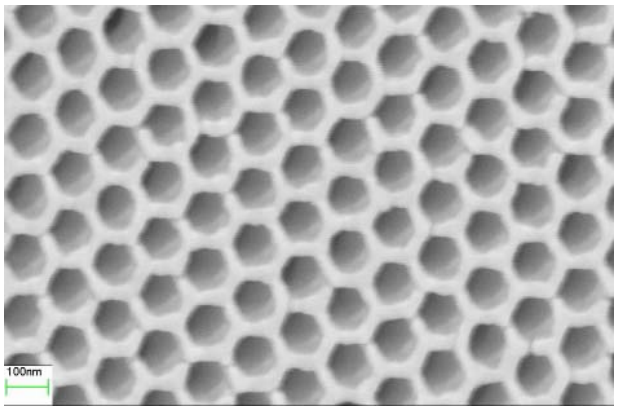

40 V

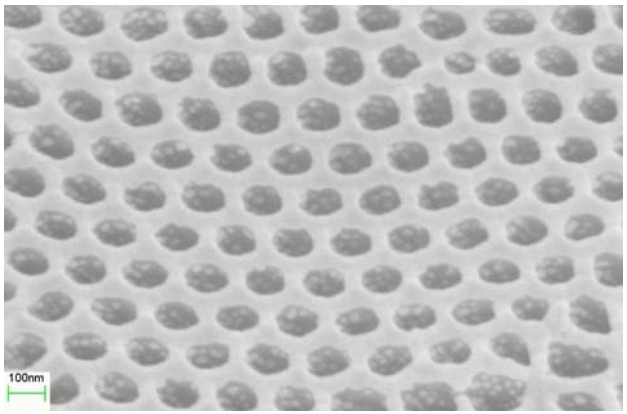

60 V

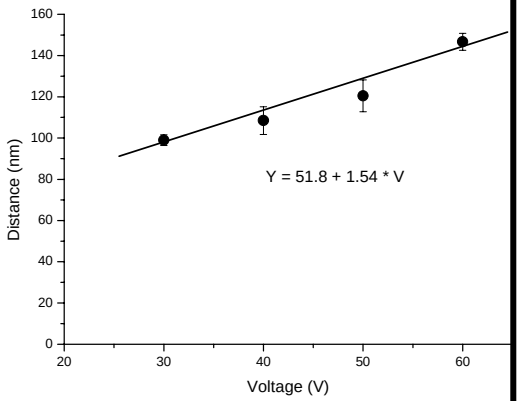

Submicrometer Metallic Barcodes

Sheila R. Nicewarner-Peña,[1] R. Griffith Freeman,[2]
Brian D. Reiss,[1] Lin He,[2] David J. Peña,[1] Ian D. Walton,[2]
Remy Cromer,[2] Christine D. Keating,[1]* Michael J. Natan[2]*

SCIENCE VOL 294 5 OCTOBER 2001

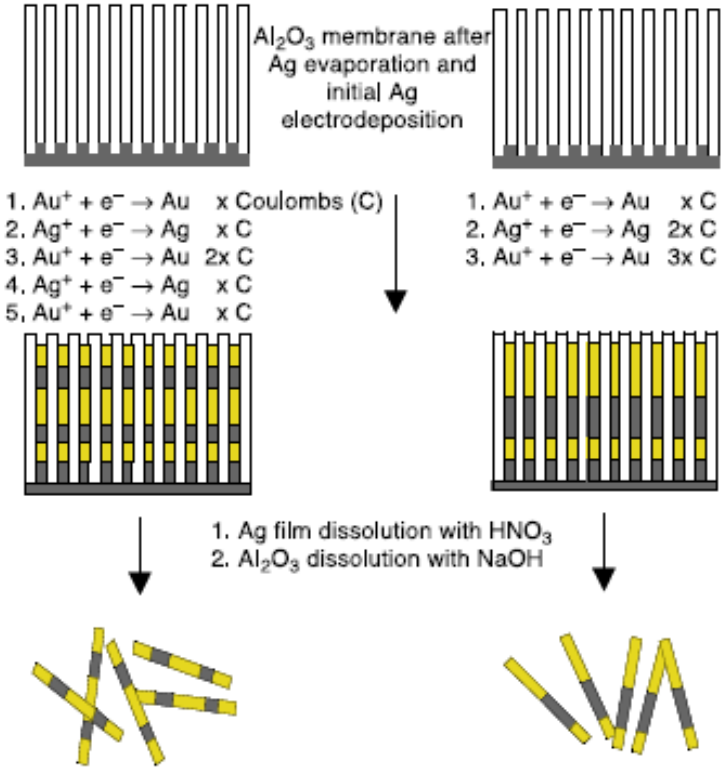

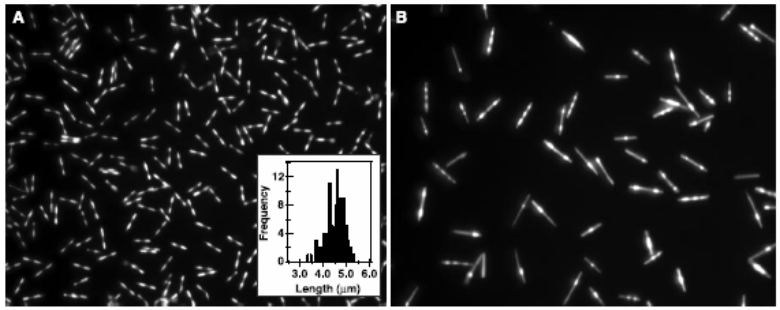

X-ray Diffraction

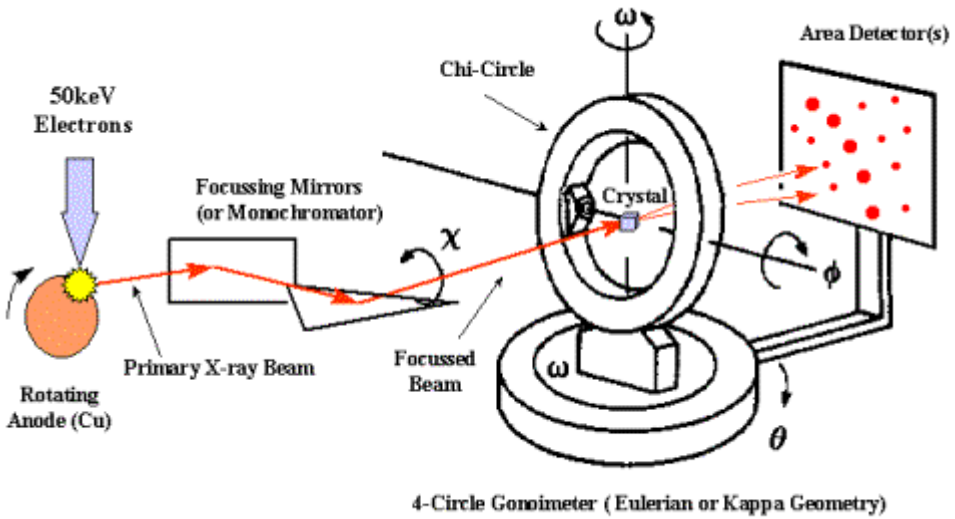

4-Circle Goniometer (Eulerian or Kappa Geometry)

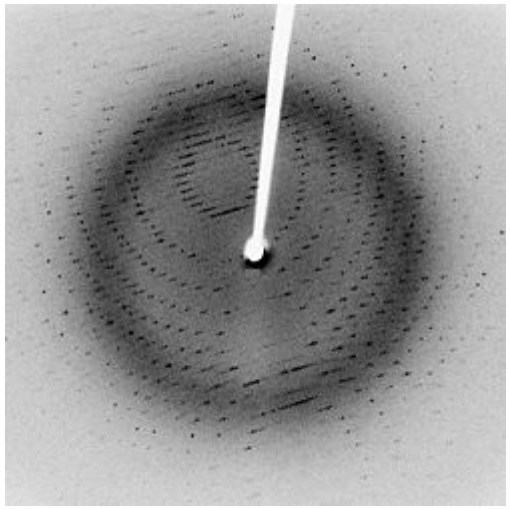

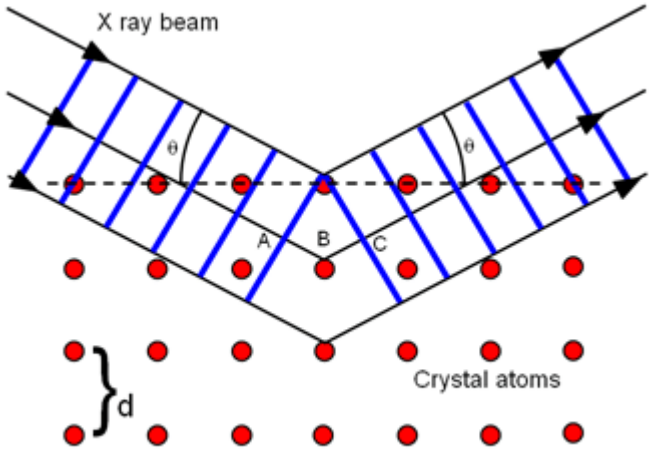

BRAGG LAW

$$2d(\sin\theta) = \lambda_0$$

where:

d = lattice interplanar spacing of the crystal

θ = x-ray incidence angle (Bragg angle)

λ = wavelength of the characteristic x-rays

Miller Index

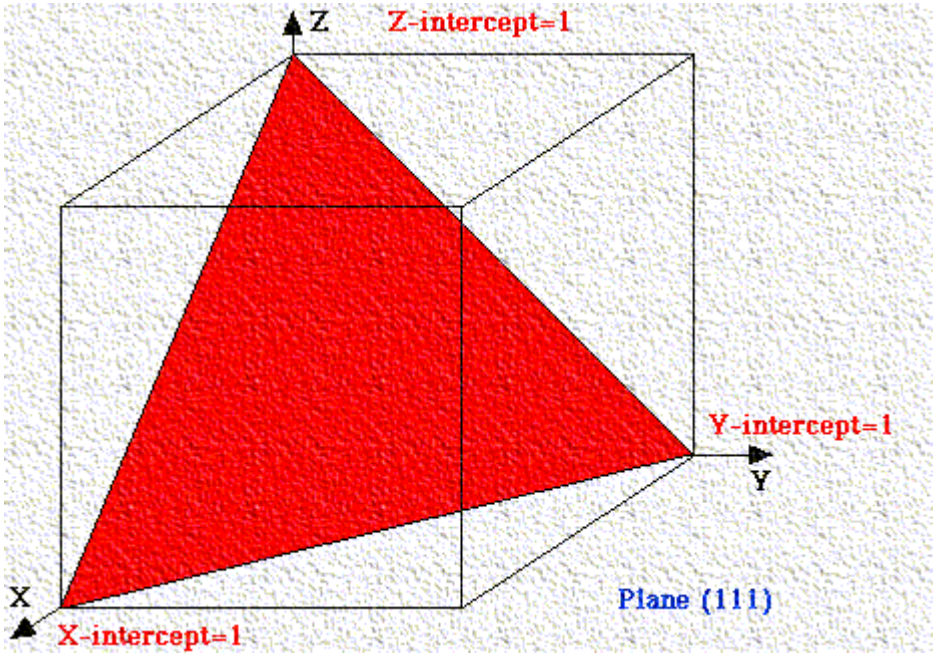

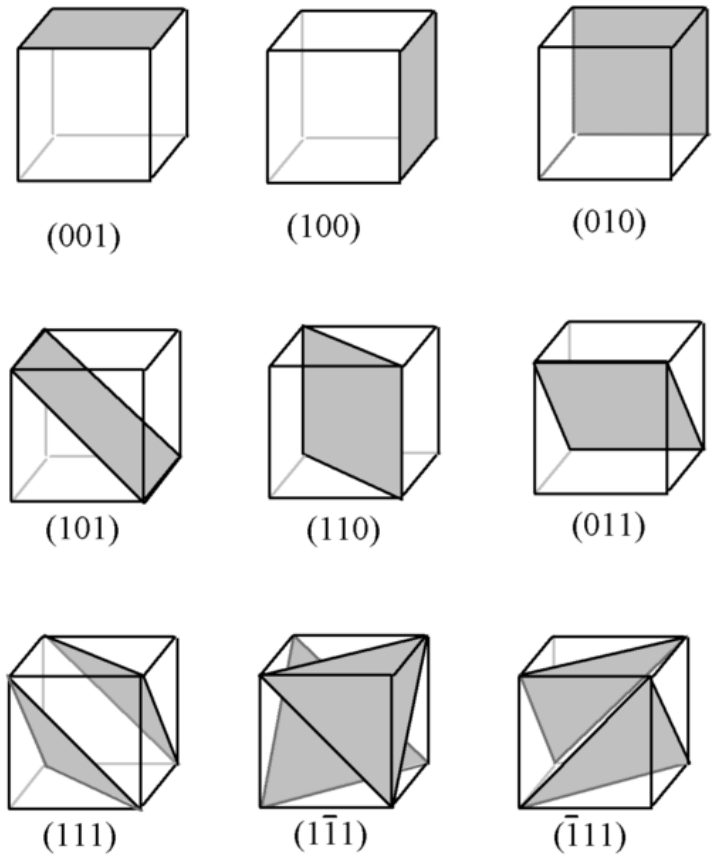

$$\ell \mathbf{b}_1 + m\mathbf{b}_2 + n\mathbf{b}_3.$$

$$(hkl) = h\vec{a^*} + k\vec{b^*} + l\vec{c^*} = \frac{2}{3a^2}(2h+k)\vec{a} + \frac{2}{3a^2}(h+2k)\vec{b} + \frac{1}{c^2}(l)\vec{c}.$$

Scherrer Equation

$$\beta_{hkl} = \frac{K\lambda}{L_{hkl}\cos\theta_{hkl}}$$

Scherrer formula:

$$t = \frac{0.9\lambda}{B\cos\theta}$$

t: particle size

B (width): in radians, at an intensity equal to half the maximum intensity.

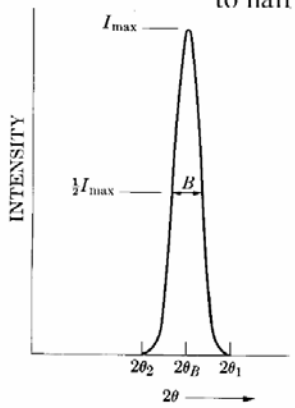

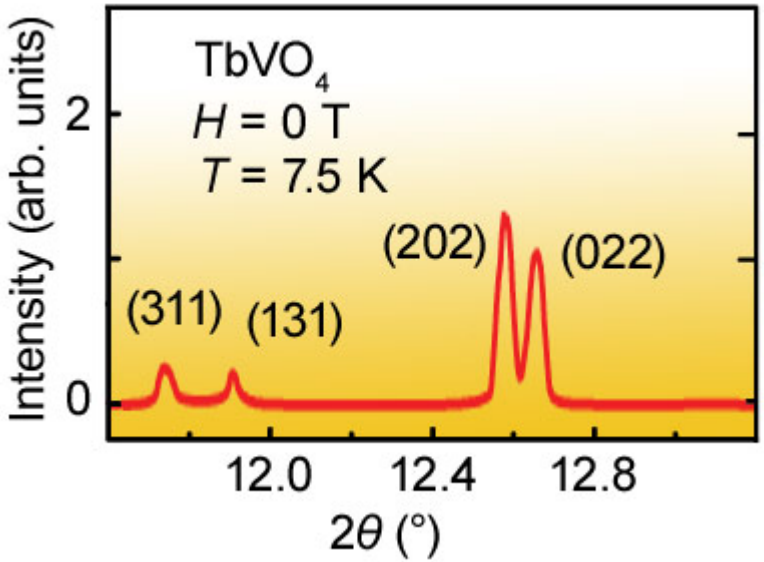

CVD Carbon Nanotube

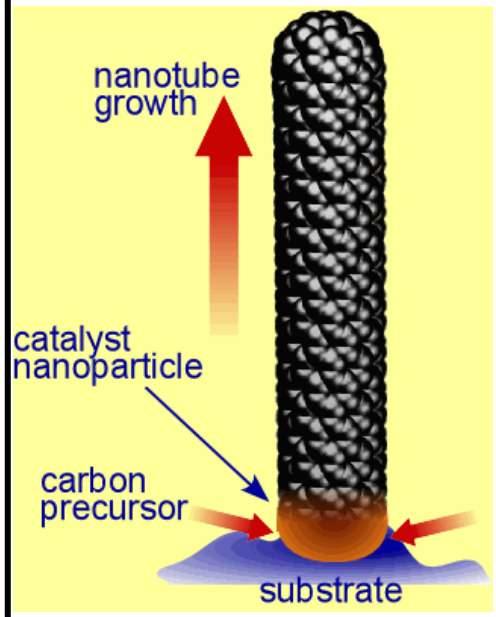

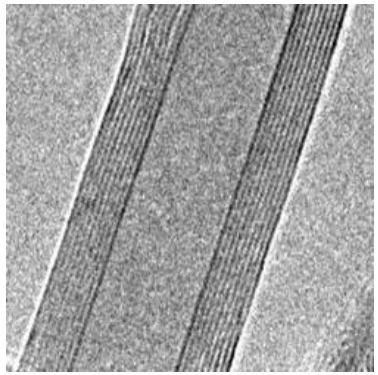

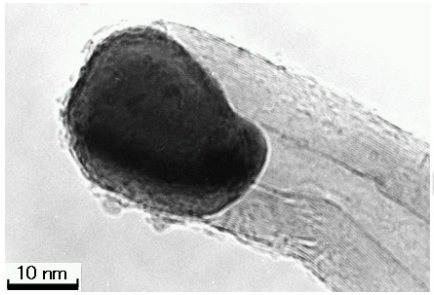

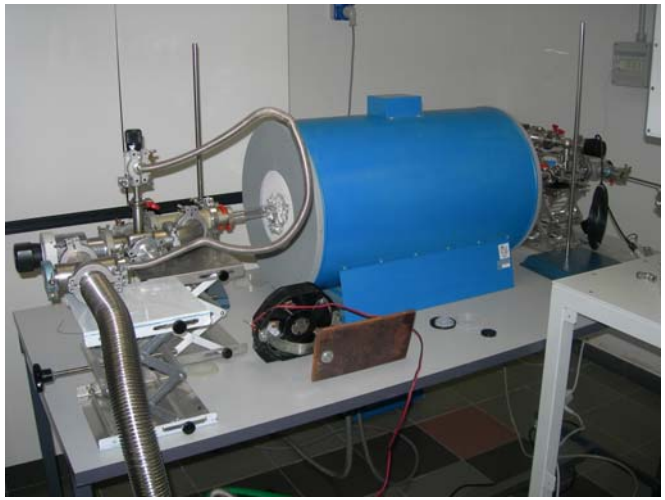

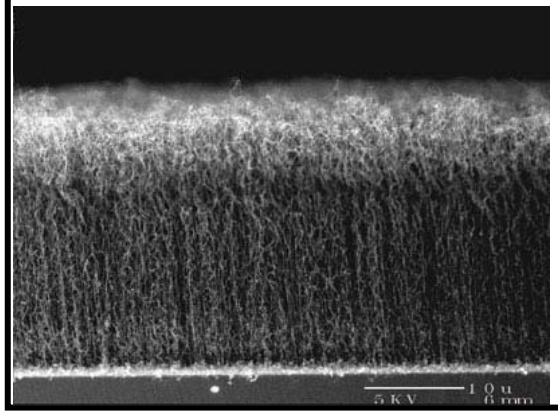

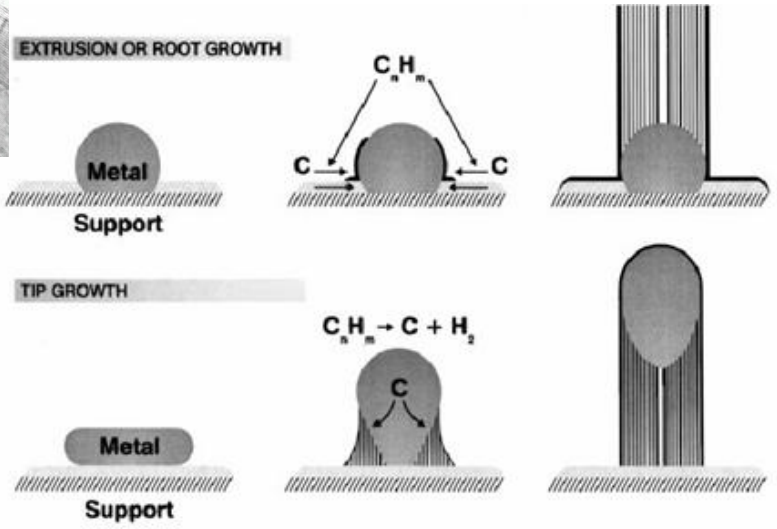

LP CVD

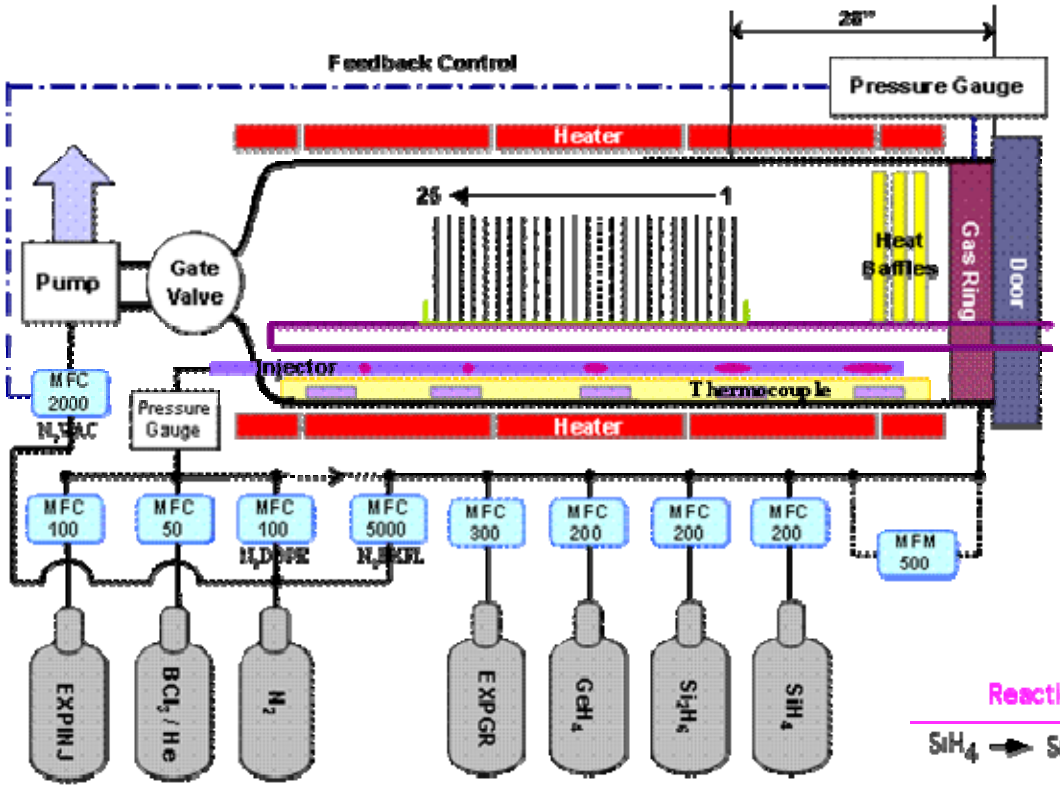

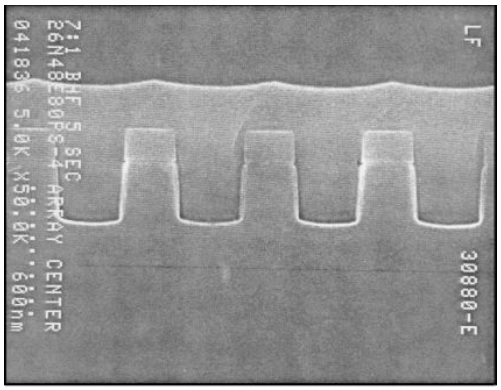

Figure 17

SEM cross-section micrograph illustrating gap filling and local planarization of a shallow-trench isolation structure, achieved using HDP CVD of silicon oxide.

Reaction	ΔH (KJ/mole)	conformality
$SiH_4 \rightarrow Si + 2H_2$	-34	spectacular
$WF_6 + 3H_2 \rightarrow W + 6HF$	-111	spectacular
$TEOS \rightarrow SiO_2 + 2C_2H_4 + 2CH_3CH_2OH$	(small)	excellent
$3SiH_4 + 4NH_3 \rightarrow Si_3N_4 + 2H_2$	-374	good to excellent
$SiH_4 + 2O_2 \rightarrow SiO_2 + 2H_2O$	-1364	mediocre

Atomic Layer Deposition

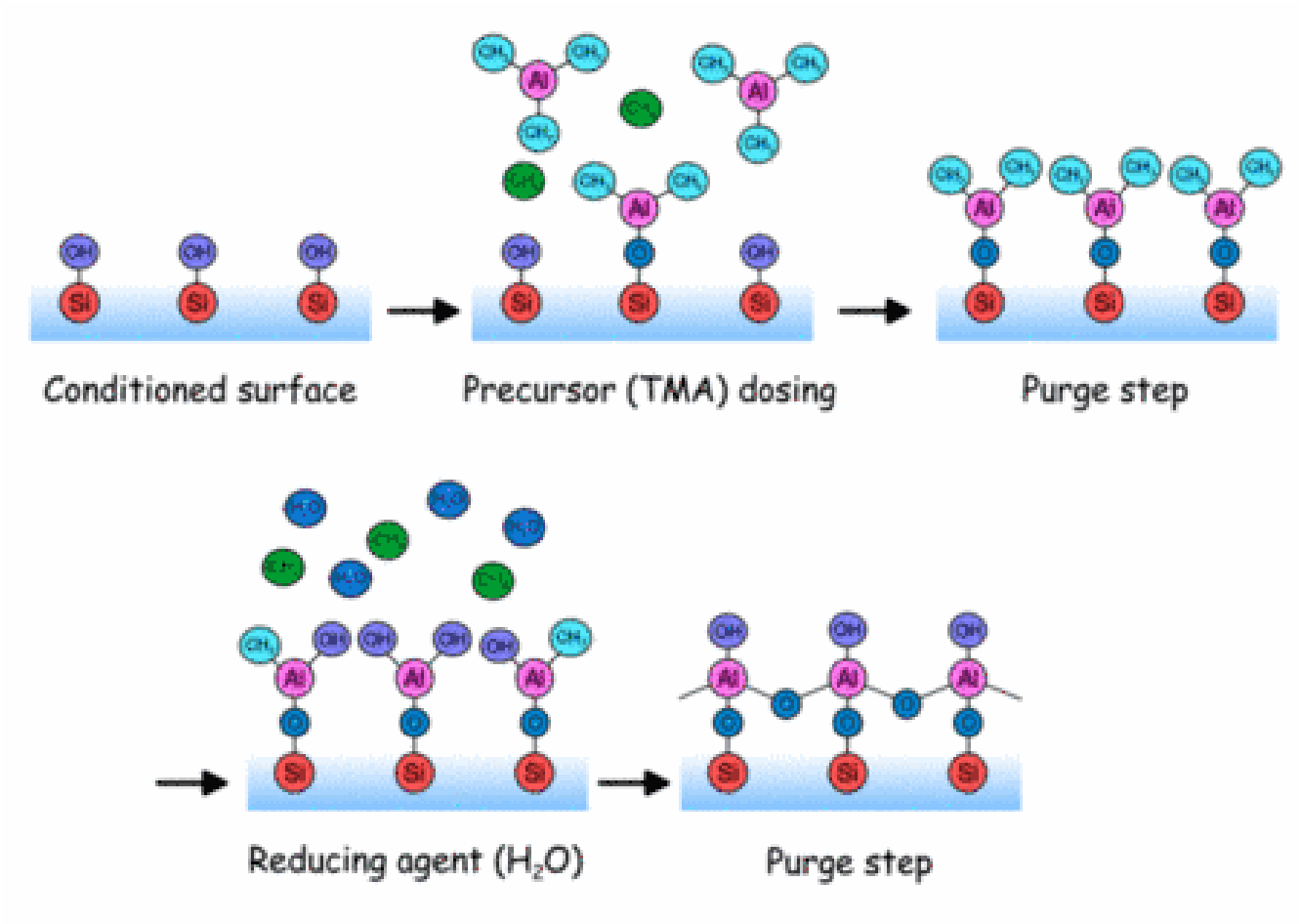

Molecular Beam Expitaxy (MBE)

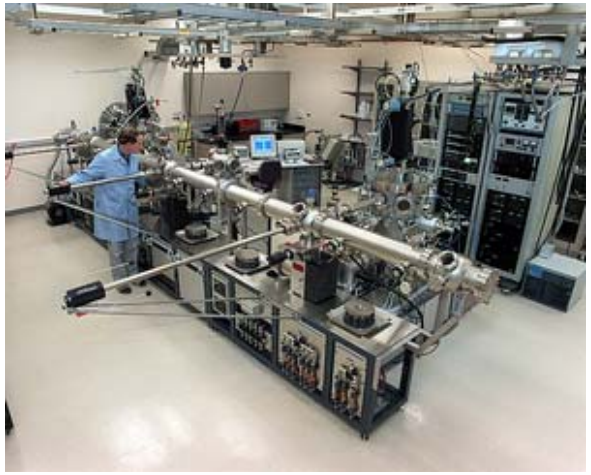

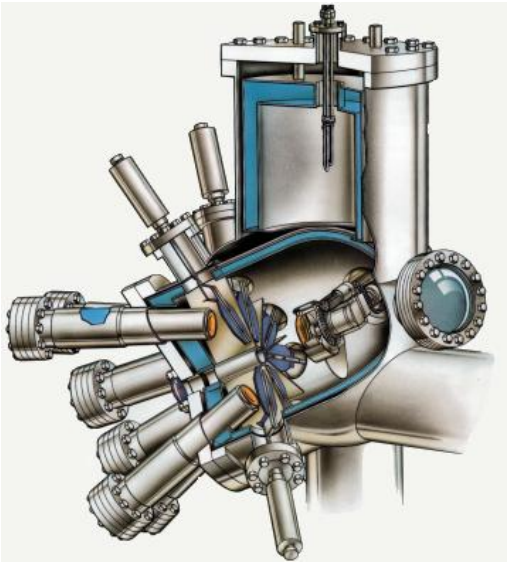

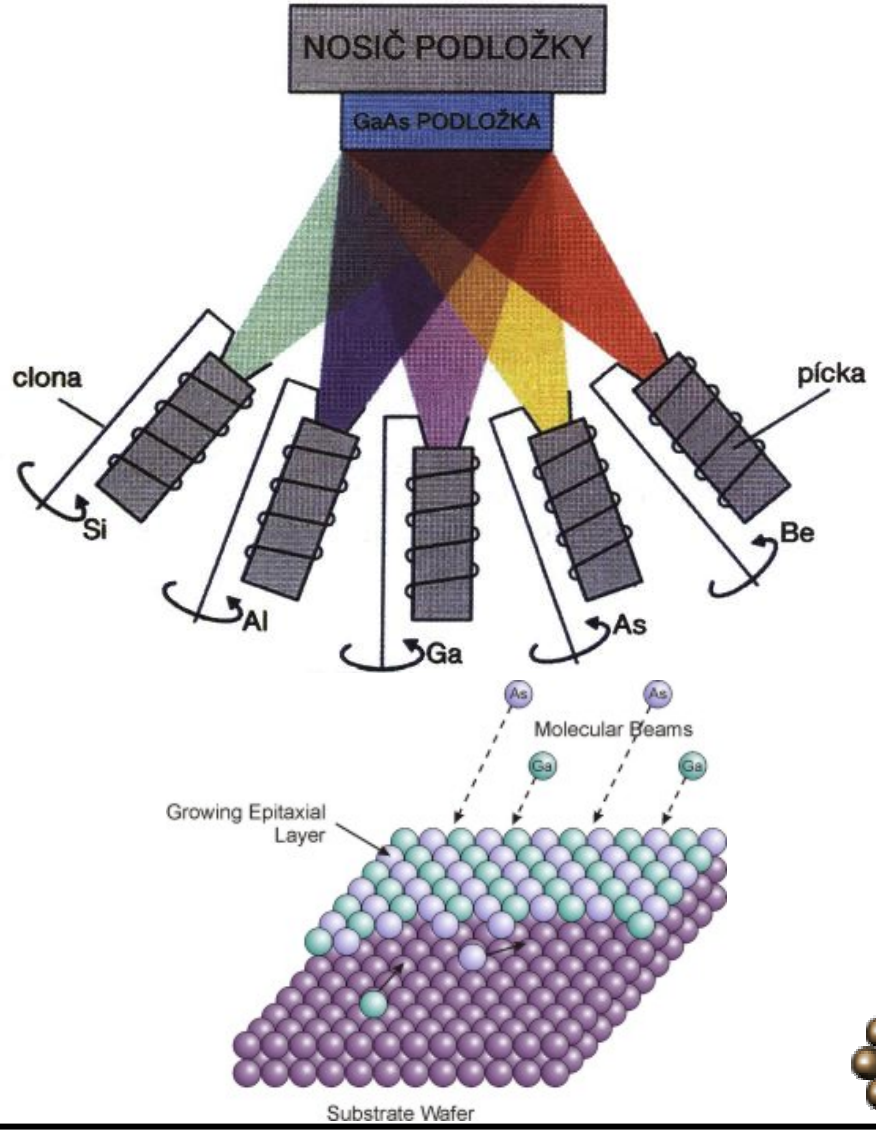

MBE

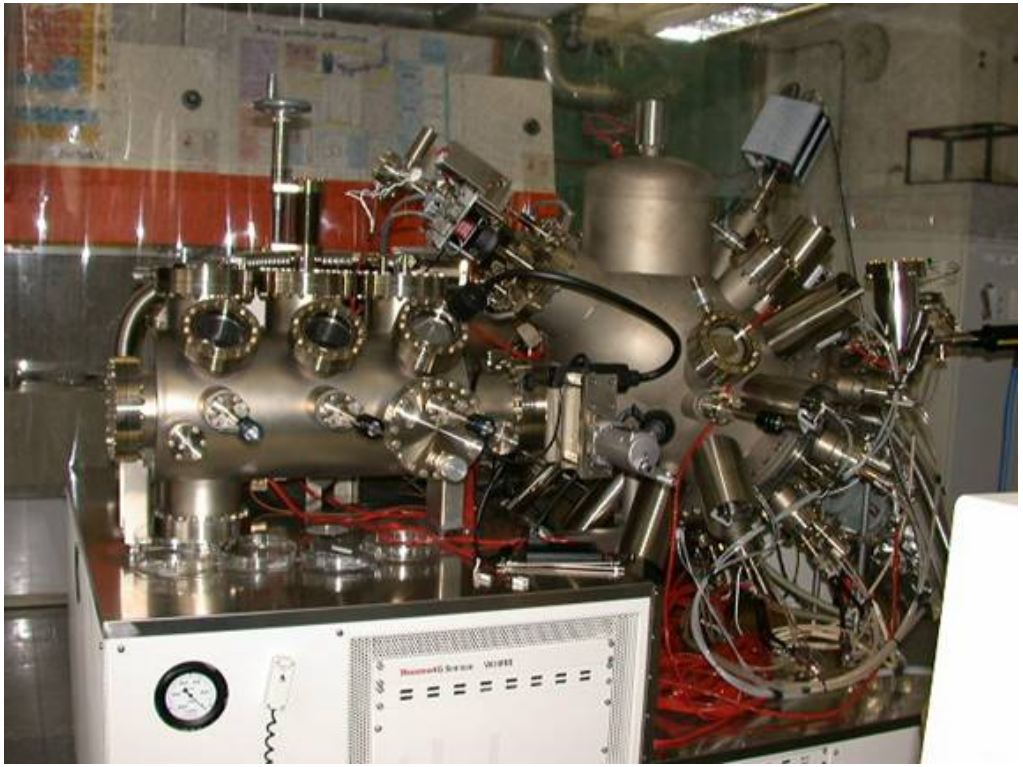

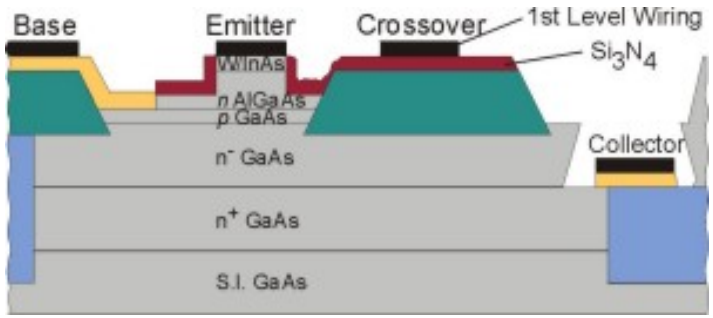
Base
Emitter
Crossover
1st Level Wiring
Si_3N_4
WInAs
n AlGaAs
p GaAs
n⁻ GaAs
n⁺ GaAs
S.I. GaAs
Collector

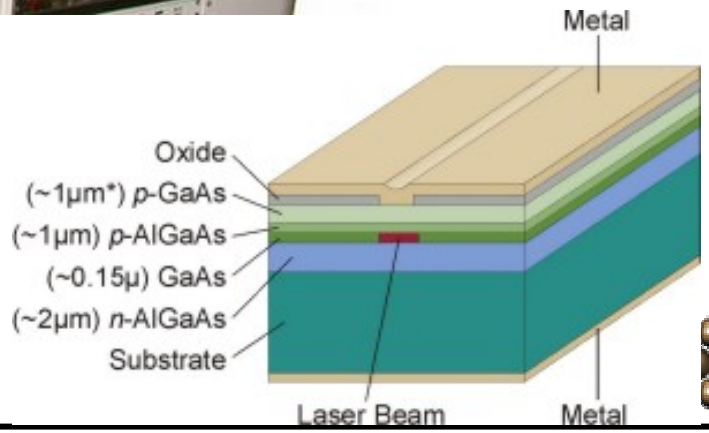
Metal
Oxide
(~1μm*) p-GaAs
(~1μm) p-AlGaAs
(~0.15μ) GaAs
(~2μm) n-AlGaAs
Substrate
Laser Beam
Metal

Template Synthesis

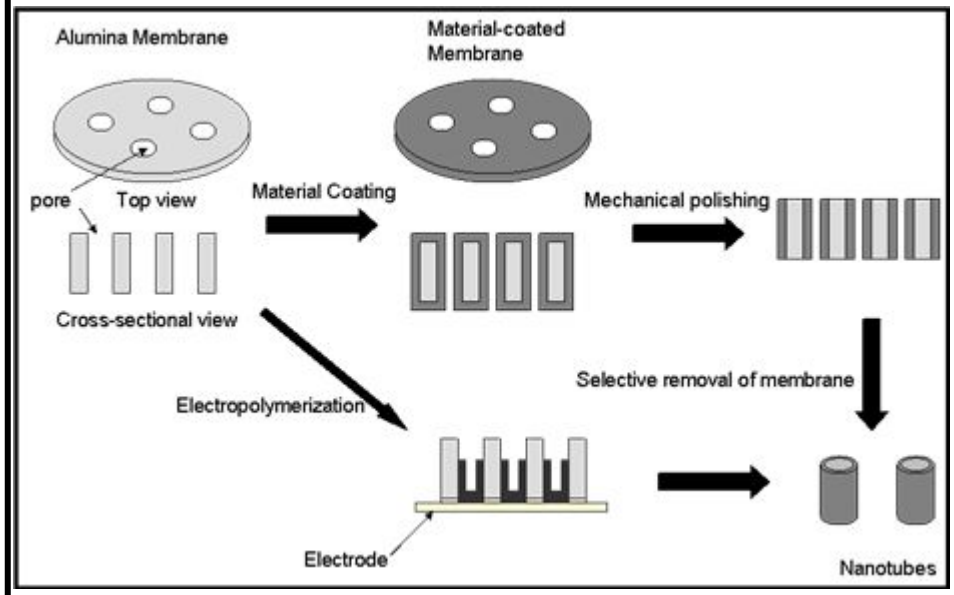

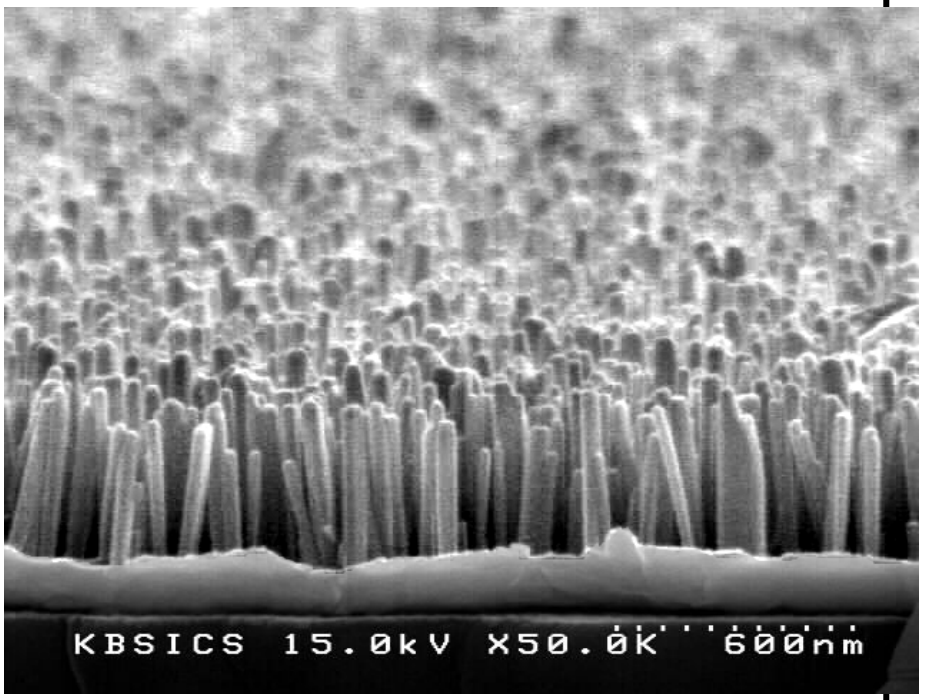

Sol-Gel

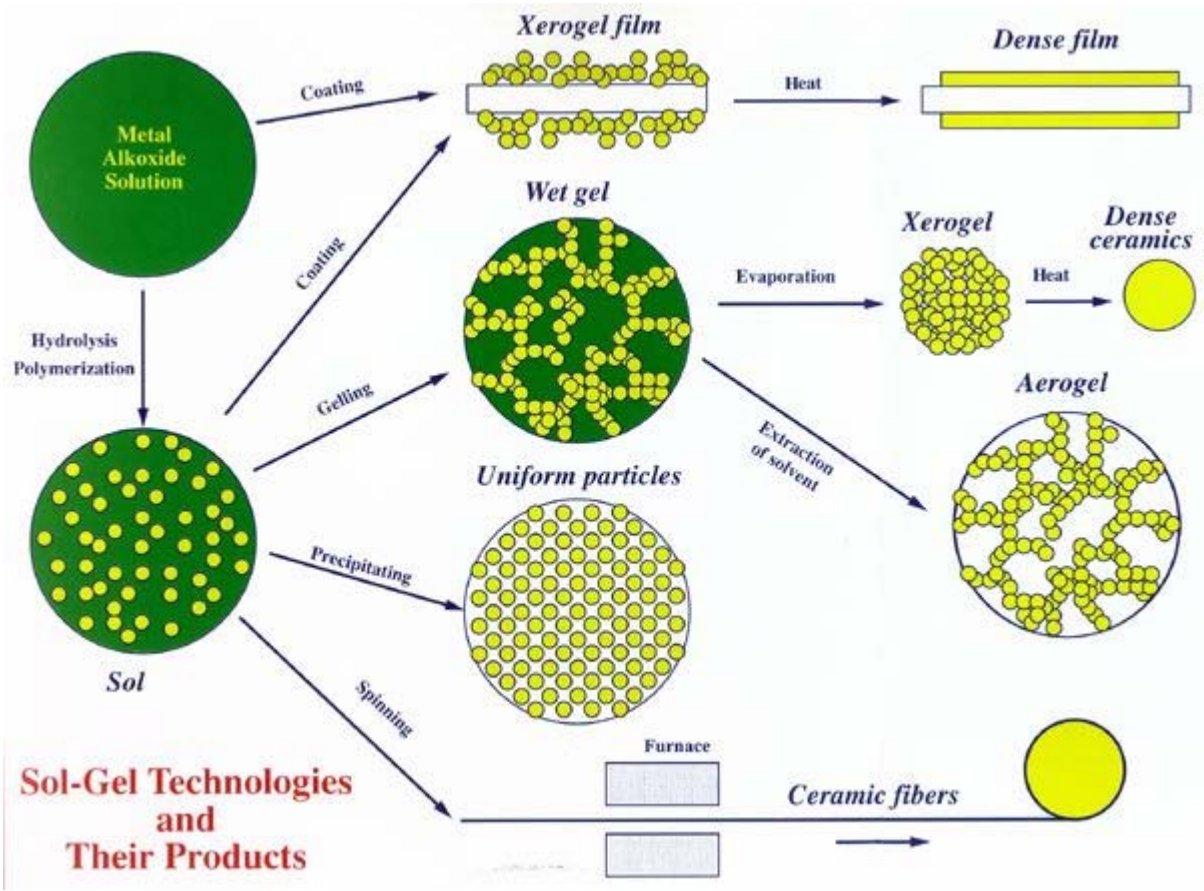
Metal
Alkoxide
Solution
Coating
Xerogel film
Heat
Dense film
Hydrolysis
Polymerization
Coating
Wet gel
Evaporation
Xerogel
Heat
Dense
ceramics
Gelling
Aerogel
Extraction
of solvent
Uniform particles
Precipitating
Sol
Spinning
Furnace
Ceramic fibers
Sol-Gel Technologies
and
Their Products